The use of non-invasive ion-selective microelectrode techniques for the study of plant development

Joseph G. Kunkel[1], Sofia Cordeiro[2], Yu (Jeff) Xu[1,3], Alan M. Shipley[3] and José A. Feijó[2,4]

[1] Department of Biology, University of Massachusetts at Amherst, MA 01003-5810

[2] Centro de Biologia do Desenvolvimento, Instituto Gulbenkian de Ciência, PT-2780-156 Oeiras, Portugal

[3] Applicable Electronics Inc., Forestdale, MA 02644, USA

[4] Universidade de Lisboa, Faculdade de Ciências, Dept. Biologia Vegetal, Campo Grande, C2, PT-1749-016 Lisboa, Portugal

***Correspondence**: J.A.F. (jfeijo@fc.ul.pt); phone +351.21.440.7941; fax +351.21.440.7970

Abstract

The non-invasive measurement of fluxes of ions and small molecules into and out of cells has become an important approach to understanding the physiology and development of plants. These methods can uncover important membrane domains of channel activity as well as link molecular fluxes with important physiological processes to which they are related. In plant cells the use of extra-cellular stepping (or vibrating) microelectrodes is of particular importance since other electrophysiological methods (e.g patch-clamp) are of difficult or limited use due to the presence of an external cell wall. Of particular impact, the use of ion-selective microelectrodes has been pivotal to characterize ion-driven processes in a number of cells and organs. The strategy of measurement and analysis is crucial in applying this technology and it is important to explain the underlying theory and methods by which these measurements and analysis are accomplished. Here we describe some of the physical and technical foundations of the method, and review some applications to plant systems in recent years.

Ion dynamics in plant development

Ion fluxes across membranes are known to have important biological roles. They exert their effect by two means: generating electrical potentials and fields and changing the local ion concentrations, thus affecting the physiological processes that are dependent upon them.

Electrical fields exert force on charged particles, from molecules to organelles and this has been proposed to lead to the movement of membrane proteins or cytoplasmic vesicles by field orientation, electrophoresis or electro-osmosis. On the other hand, cells react to the ions that carry these currents, many of which act via signal transduction pathways. If these ions have a catalytic or regulatory function, the biochemical consequences of any change in their concentration can be enough to trigger a response (Harold and Caldwell, 1990; Feijó et al. 2004). Furthermore, accumulating evidence has shown that polarity, morphogenesis and many developmental steps in plant cells are defined by an intricate network of processes that often include ion distribution and concentration as major correlates. These phenomena are available for experimental manipulation and measurement during which we can seek evidence of their causal relationships.

The molecular basis of ion fluxes in plants

Ionic equilibrium in plant cells is achieved, on one hand, by the maintenance of an electrochemical gradient by proton ATPases on the plasma membrane (P-ATPases) and, on the other hand, by the flux of other ions, namely potassium, calcium and chloride through ion channels and transporters.

Turgor and volume regulation, two crucial parameters in plant physiology and development, are a good example of processes that are strictly dependent upon ion regulation. Intra-cellular pressure in plant cells is achieved and maintained by the intra-cellular accumulation of ions and solutes, and their partition and sequestration in different osmotic biochemical forms in the vacuole (ex. formation of salts or polymers). The turgor pressure thus created is required for many physiological processes, including cell expansion and elongation, gas exchange and transport of ions and solutes. The fact that there is an active control of turgor pressure by ion and solute movement through the plasma membrane and the tonoplast also implies a fine regulation of the ion dynamics in order to achieve and maintain the necessary conditions for the transport processes in the vacuole leading to cell pressure regulation.

Pivotal in the regulation is also the activity of the vacuolar proton ATPases (V-ATPases), much different from their plasma membrane counterparts both in structure and mechanism. Vacuolar pyrophosphatases (PPases) are a third active transport party in the system. The coordinated action of these three pump systems maintains the cytosol at a fairly constant and neutral pH, while keeping both vacuole and external apoplast acidic.

These pumps are the active source of energy for a number of channels and transporters that have been both identified by physiological or electrophysiological methods (e.g. Sanders and Bethke, 2000; Taiz and Zeiger, 2002; Blatt, 2004), and that are now well characterised as specifically expressed in a number of tissues, evidenced by accumulating data on transcriptomics (e.g. Pina et al., 2005).

The particular ionic environment created by these conditions is cause and consequence of the ion fluxes across the cell's membranes, requiring tight regulatory

mechanisms that keep calcium concentration low, potassium high and a neutral pH, among other homeostatically regulated concentrations (reviewed by Feijó *et al.* 1995; Holdaway-Clarke and Hepler, 2003).

The study of ion dynamics in plant cells is therefore of the utmost importance and has been the focus of many research groups. In this context, several labs have taken advantage of these non-invasive microelectrode techniques, in particular scanning ion-selective probes, since they have become available (Jaffe and Levy, 1987; Kühtreiber and Jaffe, 1990). Some technical insights and the main results of its use in single cells are outlined in the following sections.

The scanning probe: technical advantages and disadvantages

In the past, we reviewed the application of both voltage sensitive and ion-selective probes for the scanning of membrane domains underlying the development of plants, with special emphasis on a very specialised cell, the pollen tube (Shipley and Feijó, 1999) (fig. 7, C,D). To date, the pollen tube is probably the best-studied system in terms of ion fluxes, and the matter has been reviewed both for its occurrence and biological meaning (Feijó et al., 2001, 2004; Holdaway-Clarke and Hepler, 2003). The reason for this specific cluster of applications lies in the absence of real alternatives to an extra-cellular scanning probe for use with plant cells. The analysis of ion fluxes in living cells has been accomplished through the use of relatively invasive techniques such as impalement and patch clamp. These later invasive approaches usually allow one independent sample location per cell. Further sampling proceeds at the risk that prior sampling had an effect on the cell sampled. Although results from this technique have been remarkably important for the characterization of ion channel properties and activity for developmental studies in plants, it is

compromised by serious disadvantages. Since access to the plasma membrane is necessary for the formation of a tight seal between the membrane and the patch pipette (giga-ohm seal), the plant cell wall has to be either enzymatically digested or mechanically removed, creating protoplasts. Both processes can alter plasma membrane properties, namely activity of membrane proteins, and more importantly induce a condition of stress that will likely hinder many underlying physiological processes. Moreover, the success rate of giga-ohm seal formation in plant protoplasts is generally low which is probably caused by incomplete cell wall removal or immediate regeneration of a new cell wall. The use of extra-cellular vibrating or stepping probes, being totally non-invasive methods, adds an important edge to the study of living cells, if and when the signal-to-noise ratio allows for its use.

The non-invasive scanning probes have gone through a series of transformations in use by several investigators. We describe here lines of development that we find to be particularly useful and instructive for future studies.

The original vibrating calcium-selective electrode recording system was built, for the initial use of Jaffe and Levy (1987), as a direct coupled (DC) device by A.M. Shipley and C. Scheffey at the National Vibrating Probe Facility, Woods Hole, MA.

The head stage used an AD515L chip with a 10X gain fed to an AD524 amplifier set to 100x gain with a DC offset control to cancel the Nernst Potential on the microelectrode. All measurements were referenced to an Ag-AgCl wire in a 3M KCL salt bridge placed at a far away position, millimeters away from the artificial calcium source. The microelectrode was vibrated at frequency of 0.5Hz using a bench-top square-wave oscillator signal damped with an R/C network to smooth the vibratory movement of the microelectrode.

This original design was programmed for a Digital Equipment Corporation model PDP 1123 computer using a 12 bit A/D card. The program was written in Pascal by Scheffey and it used a 60 Hz sampling routine to filter out line noise. This system measured the actual voltages across an ion selective Liquid Ion Exchanger (LIX) membrane in the tip of a microelectrode and positioned with a Starret 3D manual micromanipulator near an artificial source of calcium. Later the DC coupled device was abandoned for a time and a capacitor coupled (AC) device, introduced as described by Kuhtreiber and Jaffe (1990), which "vibrated" between and paused at two extremes of a straight path. The system was controlled by a PC based Visual Basic computer program DVIS originally written by Wiel Kuhtreiber, allowing the capacitor in series with the microelectrode to measure the difference in voltage experienced by the LIX membrane. Positioning was done with Burleigh piezopushers driven by an oscillator circuit. This AC design does not measure the actual voltage at the points of measurement and has efficiency properties based on both the LIX used and the circuit's capacitor that accumulates the voltage change. With a capacitor, the efficiency of the system varies depending on the magnitudes of voltage change measured. While paused, a short quiet-time was observed to allow the LIX to stop wobbling and then the ion probe measurement of voltage change was taken. This self-referencing protocol involved a continuous oscillation in this manner. However the probe takes a few oscillations to overcome a hysteresis and become stable and then it accumulates a rolling average of the cyclical measurements. Hysteresis is a phenomenon where a circuit's current properties depend upon its past history. When a capacitor starts out it is uncharged; as it is oscillated in a field then its first oscillation starts with no charge and a few cycles of oscillation (discharge in one direction and recharge in the opposite direction) must occur before the charge on

the capacitor has a symmetrical history comparing the opposite polls of oscillation. Thus, at least the first hemi-oscillation must be dropped as not equivalent to the next hemi-oscillations. In addition the early approach of using a rolling average creates statistical and instrumental strategy problems. Notably, the first available stable datum from this approach comes after the $k+1^{th}$ oscillation, where k is the rolling average base number of averaged oscillations. However, this protocol contributed to several important papers on tip growing systems (Kuhtreiber and Jaffe, 1990; Schiefelbein et al., 1992). At this point a division in measurement philosophy occurred and one branch of investigators returned to the DC device because of its potential as a more comprehensive approach and its focus on direct measurement that promised to be easier to calibrate. Table I lists the dynamic efficiencies estimated for the DC coupled electrodes listed which were achieved by using the continuous stepping approach (Step efficiency). These efficiencies were improvements over those achieved with the AC devices and were listed for informational purposes on a website (www.bio.umass.edu/biology/kunkel/nvp_cali.html). Unfortunately this table of efficiencies was assumed to apply to all oscillating probes and often AC device results were published without benefit of there own efficiency estimates. This is a major problem for the AC devices since there is no investigator who has taken the responsibility for developing an adequate approach to establishing their dynamic efficiencies. In the few measurements of the dynamic efficiency of the calcium LIX using the AC devices driven at identical Hz at the National Vibrating Probe Facility, the dynamic efficiency was substantially lower than with the DC amplifier. Using the DC device and through software improvements to the DVIS software it was possible to eliminate rolling averages that created correlations between adjacent measurements, a bad experimental design. Rolling averages were replaced with

statistics on independent unit measurements and this approach was used in further tip growth studies (Feijó et al., 1999; Cardenas et al. 2000; Zonia et al., 2001, 2002; Holdaway-Clarke et al., 1997). Since the idea is to detect specific ion concentration as a function of DC voltage change on a LIX microelectrode it is crucial to detect the actual DC voltage at each extreme of the vibration or movement excursion of the microelectrode. Fundamentally these systems are concentration meters that derive ion flux or movement as a function of the local ion concentration difference measured between two positions close to a membrane. To accomplish this, the SIET system was developed (Shipley and Feijo, 1999). A major change in measurement protocols with this DC device allows for more rapid-, multidimensional- and multi-probe-measurements. ASET (Automated Scanning Electrode Techniques) software, developed by Eric Karplus, (Science Wares, Falmouth, MA) established the sampling-rule approach to measurement. The sampling rule defines a set of unit measurements that can be as simple as a stationary measurement at one point with one probe, or as complicated as 3-dimensional flux measurements involving stepping in the micrometer range of differential distances to measure differential concentrations with multiple probes, whether voltametric, amperimetric or both. Statistics on sampling is accomplished by replicating sampling rule unit measurements using standard experimental designs and controlling the pattern of unit measurements using interactive software-defined patterns of sampling sites. Complications of hysteresis are avoided in the DC sampling rules because the symmetry of oscillatory (differential) data does intrude on the collection process. As a result, a substantial improvement of the dynamic efficiency is achieved for the DC sampling rule approach for all LIXes tested as is indicated in Table I. It must be emphasized that the individual investigator is responsible for establishing the

dynamic efficiency of the electrodes used within the context of the sampling rule applied (cf. Table II). Dynamic efficiency will vary with the length of waiting time for LIX wobble to subside, length of probe integration of the signal, the properties of the LIX used and factors specific to the LIX and electrodes and sample bath used. For instance, the strength of the buffer can dramatically influence the apparent flux of protons (Faszewski and Kunkel, 2001). The 100% dynamic efficiency achieved with the DC sampling rule approach (Table I) applies only to low- or un-buffered samples. In low buffered situations one must wait until the tissue metabolism has secreted enough protons to clear the local culture media of effective buffer, otherwise the buffer extinguishes protons as they are secreted and the probe has effectively nothing to measure (Kunkel et al., 2001). Use of traditional bicarbonate buffered culture media such as Holtfretter's solution will result in a substantial loss of efficiency (eff = 63%) in measuring protons. Doubling the bicarbonate buffer in the Holtfreter's results in a reduction in efficiency to 43% (Faszewski and Kunkel, 2001). Reviewers are cautioned to ask of scanning probe manuscripts they review "Where is the dynamic calibration?"

The SIET approach in general is especially suited for developmental situations that involve growth or morphogenesis of a cell or tissue. This is because the microelectrode can be non-invasively moved around in the extra-cellular medium surrounding a specimen thus allowing large linear or area scans, as well as tracking a modulating or growing sample.

These non-invasive extra-cellular methods provide complimentary information to add to intra-cellular methods using fluorescent reporting molecules (e.g. Holdaway-Clarke et al., 1997). In their most ambitious applications with adequate calibration, non-invasive ion probes can be used to integrate the relatively steady ionic fluxes

emanating from a region or unit surface area of a cell or cellular membrane (Cardenas et al., 1999, fig 8F). Often a probe has been used in a semi-quantitative way to observe relative ion flux spatial patterns focusing on temporal oscillatory patterns without calculating flux at other than the probe position in one dimension or extrapolating the flux to the cell surface (Cardenas et al., 1999; Holdaway-Clarke et al., 1997; Feijó et al., 1999, fig 8E). Ion probe calibration is more essential to its more quantitative applications in which the properties of a particular region of a cell are of interest (Cardenas et al. 1999, fig 8F), or where the measurements are of importance in relating components of a model to one another (Feijó et al., 2001). The calibrations include simple calibration of the probe according to the Nernst equation [1]:

$$\mathbf{V = V_0 - (RT/zF) \bullet \ln (H/HA)} \qquad \mathbf{[1]}$$

as well as determining the efficiency of the dynamic process of measuring the voltage difference between two points. In the later efficiency determination there is a trade-off between allowing any probe wobble to come to rest after a move to a new location, the speed of the LIX to respond to the new location, the length of data collection, repetition of the measurement and how many other points one wants to measure in an experiment. Patterns of measurements that include long movements between their starting positions require longer wait states to allow LIX wobble to subside. LIX wobble does not cause a decrease in efficiency; rather it creates random noise resulting in outlier data. For that reason, more weight must be given to wobble suppression (via longer wait states) versus longer integration time. It is always possible to trade lower efficiency for more rapid measurements in order to maximize the number of informative measurements. In any event the dynamic efficiency of a

probe needs to be established for the sampling rules chosen if the data is to be used for anything more than relativistic comparison within an experiment. The DC approach has an advantage over the AC approach in this respect. The AC approach has a symmetrical but additive loss of efficiency at both ends of the measurement cycle. As detailed earlier (Kunkel et al., 2001) the DC approach reduces the loss of dynamic efficiency by starting at an origin at which there is little or no loss of efficiency, cutting the loss of dynamic efficiency at least in half at each measurement site. DC measurement devices and protocols are a faster and more accurate measurement system than the AC approach. The DC approach also provides the user with a high gain device that can be used in a stationary way to measure flux oscillations in real time, which the AC system cannot do because of its limited frequency mode of measurement.

Stationary ion-selective microelectrodes can also be used to infer cellular activity but it is only applicable when large enough signals are being recorded, usually on large enough organs to generate sufficient detectable currents (e.g. roots). Vibrating or rather, as described above, stepping a microelectrode between two positions and measuring the DC voltage difference between the positions of the microelectrode greatly increases sensitivity and corrects for microelectrode drift as long as the stepping is much faster than the drift. This is particularly important when studying single or isolated cells that generate smaller currents than whole tissues or organs. Unfortunately the extra-cellular microelectrode used can only measure the ion concentration at points outside the cell wall of plants. However, the use of specific inhibitors for ion channels or transporters that putatively convey membrane fluxes provides clarification of the relative contribution of fluxes across the plasma membrane.

All things considered, the Scanning Ion-selective Electrode Technique (SIET) is an easy, reliable, accurate and rapid technique that can readily detect minute ion fluxes in a non-invasive way. In a number of situations, intra-cellular ion concentration and its modulation by fluxes across the plasma membrane are potentially one of the earliest diagnoses of any changes that a cell displays. Therefore, the SIET has become a useful tool for the study of biological phenomena in which spatial and temporal resolution are an issue.

For reasons outside of the scope of the present manuscript, the very same principle we describe here, with different instrumental interpretations, is used associated with various acronyms, namely "MIFE" (see chapter 3), "SERIS" (see chapter 6), and "SIET" here. In essence they all use the same basic relationship, the Nernst equation [1], which relates electrical potential to ionized compound concentrations. However the DC and AC approaches diverge in technical design that sets limits or advantages for each implementation. Self-referencing AC systems like SERIS are based on the capacitor coupled measurement of microelectrode voltage differences measured at opposite extremes of an oscillation. The SERIS system does not directly measure the voltage on the microelectrode at each point but rather records the results a software averaging algorithm accumulating the difference (delta V) between the two points by the LIX in series with a capacitor. Though SERIS can measure the presence of a flux of an ion, it is unable to accurately measure the actual strength of the flux. The SERIS approach calibrates the electrode at low gain (DC x 10) millivolt sensitivity, but makes the delta microvolt measurement (gain x 1000) via a capacitor. Since efficiency of the LIX electrode is not measured at microvolt levels, it is unable to measure the flux accurately. In the AC SERIS protocol the local concentration of an ion is assumed to be close to the background media's composition (Kühtreiber and

Jaffe, 1990) which is a logical first guess but may not be accurate in situations where the cell is actively pumping the ion of interest. This is particularly true when dealing with proton secretion where the local buffer of proton concentration must be low enough for the cellular pumping surfaces to overcome in order for an ion concentration gradient of protons to be measured (Kunkel et al., 2001). A distinct advantage of the DC based SIET approach is its use of direct measurements of voltages at each measurement point, at high gain, that are regulated by the flexible "sampling rule" at each sampling location in a data collection protocol. The sampling rule can be crafted so as to create 1-, 2-, or 3-D measurements using one ion-selective microelectrode or sequential or interleaved measurements (Table II) of multiple ion-selective microelectrodes in one or multiple dimensions (Faszewski and Kunkel, 2001). Within this well-defined "sampling rule" paradigm a calibration and dynamic efficiency of each micro-probe type can be determined and used. In addition the temporal and spatial correlations between different ion fluxes within the sampling rule unit measurement can be estimated and examined with an experimental design to establish causality. SIET probes can also be interleaved with polarographic (amperimetric) microelectrodes by a sampling rule (Table II) that extends the molecules measured beyond the current review's scope to non-ionic small molecules such as oxygen and nitric oxide.

This capability of measuring multiple ions is also critical to accurate estimation of certain ion fluxes. For instance the LIX nominally used for measuring bicarbonate is primarily sensitive to carbonate which at physiological pHs is a minority of ions present in the carbonate/bicarbonate equilibrium. In order to accurately measure the total carbonate/bicarbonate concentration one must also simultaneously measure local pH that is involved intimately in the equilibrium. In addition, many tip growth

studies use tip growth as the common factor that allows one to correlate the relative timing of internal and external ion movements (Holdaway-Clarke et al, 1997; Feijó et al, 1999; Roy et al, 1999). The sampling-rule approach is highly compatible with correlating the measurement of ion probe data with interleaved cellular and intracellular data obtained from image analysis (Holdaway-Clarke et al, 1997; Feijó et al, 1999).

Capabilities of scanning microelectrode technology

In order to establish the capabilities of particular scanning microelectrode setups and analyze the data collected with it we routinely use artificial sources or well defined model systems such as the growing pollen tube whose cylindrical shaft and hemispherical growing tip can be geometrically better understood. In that way we can objectively test the limits of a new protocol or measurement system.

The artificial point source device.

Understanding the signals one obtains by measuring standard artificial sources or sinks that provide models for the types of currents they wish to measure in living material is a recommended first step in every experiment using this kind of technology. The construction of an artificial point source or sink can use a pulled capillary shape recommended for a measurement probe pulled in multiple stages to have a bee-stinger shape (Kühtreiber and Jaffe, 1990). This is useful so that one can have the infinite source or sink bulk solution nearby the tip that represents the point source. This source (or sink) should have a tip diameter of 5-10 microns and be filled with a low percentage agarose (around 0.5%) to stabilize the filling solution of the ion or molecule of interest. A filling solution 3 orders of magnitude higher or lower

in concentration than the bathing media is usually sufficient to provide a strong point source or sink, producing a passive diffusional gradient that is easy to detect with an ion-selective microelectrode. The agarose does not provide any hindrance to the diffusion of the molecule through the tip but will stop bulk flow of the filling solution. If simulation of an electrogenically driven ion flux is to be simulated, one can include a DC circuit through this source making sure that the source components and sink are simple enough to allow the ion of interest to be a predictable component of the current to be measured. The predicted pattern of diffusing oxygen into a recessed platinum electrode surface can be seen in Figure 1A that illustrates a sagittal section through the artificial source tip and sphere of predictable oxygen concentration. The equations for this diffusion pattern are given by Schneiderman and Goldstick (1978). This very predictable source or sink model is ideal for practicing with a probe on a known strength and shape diffusion source. The results of measuring the flux emanating in the three directions, x, y and z, from a point source in a grid of points in a YZ plane tangent to the sphere of molecules diffusing from a point source tip such as in Fig. 1A is plotted in various ways in Figures 1B,E,F. Planar contour plotting functions of grid data (Fig 1E) are available in many computational software packages such as MathCad, Matlab, or R. The contour plot is useful in viewing the expected reversals in the components of flux, $\mathbf{J}_y$ and $\mathbf{J}_z$, but the unimodal probe centered contours of $\mathbf{J}_y$, as measured in the ZY plane when the probe passes through the flux plume diffusing from the point source. The characteristic reversals of flux components, as the probe passes high and low in the Z dimension, emanating from the source tip can also be seen in linear plots, Fig 1E, of the $\mathbf{J}_y$ data from Fig 1D. A more intuitive stereo view of total flux vectors, Fig 1B,C, requires use of software packages such as Mage, able to represent points in space and provide

stereo pair views of that data. It is valuable for an investigator to be aware of the total flux vectors involved at each point measured when one is plotting 1- or 2-dimensional representations (e.g. Fig 8A-C) of those vectors. In some cases a vector can represent a small local 1-D component of a larger 3-D flux associated with an adjacent localized point source or sink. Familiarity with the measurement phenomena, solid geometry and distance, inherent in Fig 1 is critical to understanding fluxes measured from natural sources.

For testing multiple-probe arrays one can devise gradients of each molecule of interest eminating from a single point source. For instance, to create a joint point source for protons and carbonate and point sink for oxygen, one can craft a small capillary with gaseous CO_2 forced to the tip presenting a small gaseous interface that releases CO_2 which associates with the water to form a point source of bicarbonate, carbonate and protons. In addition the pure CO_2 bubble provides an infinite sink for dissolved oxygen. This artificial source has been used for testing multi-probe pairs such as HCO_3^- and protons (Faszewski and Kunkel, 2001) or protons and O_2.

Calibrations of probes using particular sampling rules

Each LIX microelectrode has an efficiency of flux measurement dependant upon the time it takes to settle to a new voltage level at a new ion concentration. Calibration of a DC system in solutions of known concentration is a meaningful measurement of LIX responsiveness and relates directly to how the electrode will be used in measuring gradients. Presented with detecting a steady state ion flux from a point difusional source, Fig 1A, is a matter of waiting long enough at a given sample position with sufficient gain to record an accurate ion concetration measurement, then moving to another position and remeasuring. The flux between the two points is a

simple matter of calculating the dC and the dx of equation [6] as explained below. During most live experiments however one does not have the luxury of a steady state source and waiting for long periods at each measurement point. A pollen tube grows while one is watching it and it presents oscilating fluxes to measure. Irespective, with the SIET system, LIX microelectrode drift can also be recorded at high gain to provide the user with a recorded time period and magnitude of the drift being experienced. This allows the experimentalist the luxury of designing a measurement scheme with total knowledge of the measurement challenges to overcome.

There are two types of calibrations that must be made on each probe type before they can be used for practical live measurement. All are based on the Nernst Equation [1]. One is the static calibration similar to calibrating a pH meter (Fig 2A) estimating the slope, **A**, of the voltage vs log [H] plot using two standard solutions, **a** and **b**, [2, 3]

$$\mathbf{pH_a - pH_b = log[H^+]_a - log[H^+]_b = (mV_a - mV_b) / A} \quad , \qquad [2]$$

$$\mathbf{A = \Delta mV/\Delta pH} \quad , \qquad [3]$$

or a multipoint calibration by estimating the slope of the linear regression [4],

$$\mathbf{V = B + A \bullet log[H^+]/eff_s \approx B + A \bullet log[H^+]} \quad , \qquad [4]$$

using three or more of the standard solutions as seen in Fig 2A.

The slope, **A**, and intercept, **B**, determined for the probe based on the set of standard solutions can be used to estimate future concentrations, cf.[5], measured by that electrode, at least within the range of those standards used:

$$[H^+] = 10^{(A - V*eff)/B} \approx 10^{(A - V)/B} \quad [5]$$

Experience shows that future replacement electrodes made with the same LIX and electrolyte backfill can be checked for an appropriate voltage with a single point calibration, namely the bathing solution in use. Thus the estimation of the concentration at the origin of a unit measurement, C_o, is made using a static calibration curve similar to [5] for which there is close to 100% efficiency as there is with a pH meter. The other more important calibration (critical in that it is less likely to be close to 100% efficient) is a dynamic calibration which may be necessary for adequately estimating C_x which is the concentration measured after the quick move to position x. It depends on the LIX used and the imposed sampling parameters such as the length of the LIX column, the wait before measuring and the length of the measurement phase, which jointly give rise to the probe dynamic efficiency (Fig 1D) which when divided into the observed microvolt difference approaches predicting the true microvolt difference that is critical to calculating the accurate flux (Fig 1G).

$$\mathbf{J = D \bullet {}^{dC}/_{dx} = D \bullet {}^{(C_x - C_o)}/_{dx}} \quad [6]$$

Thus the loss due to dynamic inefficiency would exhibit itself in the estimation of the C_x component of dC. The probe is usually allowed to sit at the origin where C_o is measured for a wait state long enough for the probe to have reached close to its optimum voltage (i.e. ~100% efficient) which can be applied in equation [5] to obtain

C_o. However when the probe is moved dx units to its position for measuring, C_x, it is the voltage difference between the origin and dx that is the objective to be estimated in that move but it is sometimes necessary to take the voltage reading, V_x, at the dx position (Fig. 2C) before the probe has come to equilibrium. A dynamic loss of efficiency can occur in measurement of V_x, underestimating the voltage difference over the short distance from the origin. We must estimate the inefficiency in measuring this microvolt difference or a systematic underestimate of flux will occur every time the sampling rule is applied. One usually wants to take the V_x measurement at dx quickly in order to avoid any drift in the probe's voltage, since its measurement at the origin, and also quick enough to allow more sampling rule unit measurements to be made to make the overall experiment data rich while a living source remaines healthy. With the trusted, relatively stable point source the voltage at each point, **r**, away from the known source can be measured with the probe in static positions. Then, **V** vs **1/r** is plotted, a curve is fit to it and the expected voltage difference for the small extra move is calculated by interpolation between the measured points. In the same time frame as the static measurements are made, the voltage difference for a rapid dx move can be directly measured dynamically in real time. The difference between the measured and calculated voltage difference provides an estimate of the dynamic inefficiency of that phase of a sampling rule. This artificial source dynamic efficiency estimate provides the efficiency to use in correcting future experimental measurements of voltage differences. For a rapidly responding LIX such as the proton LIX there is almost no dynamic loss in efficiency in the measurements of the secondary voltages at dx, dy or dz and thus a 100% efficient estimate of a 3-D flux can be assumed, Table I. This high or 100% dynamic efficiency is not true for the older continuous AC vibrating or SERIS methods in which efficiency is lost at each

end of the microelectrode oscillation, leading to further losses of efficiency for the proton electrode (Kunkel et al., 2001).

When pure forces of diffusion are at work and vibrations and disturbances of the point source can be suppressed, the concentration of ions diffusing from a point source such as displayed in Fig 1 can be modeled as a hyperbola:

$$\mathbf{C_r = C_b + K/r,} \qquad [7]$$

where $\mathbf{C_r}$ is the concentration at radius r and K is a proportionality constant which includes the diffusion coefficient; $\mathbf{C_b}$ is a background concentration which the hyperbola is asymptotic to as a background solution. Unfortunately ***r*** is not the distance to the point source but rather an hypothetical point up the point-source-shaft that corresponds to the infinite source end of the hyperbola at which r is zero. This point can be estimated, providing a straight-line theoretical curve of expected concentrations or microvolt differences at given diffusional radii. Points very close to the orifice of the point source do not conform to this linear curve and often need to be dropped from the data. It is in such a context of expected microvolt differences that one can estimate the dynamic efficiency, $\mathbf{eff_d}$. This dynamic efficiency is used in an equation [8] for estimating $\mathbf{dC}$,

$$\mathbf{dC = C_r - C_{r+dx} = C_r - 10^{(mVr + \mu Vdiff/1000*eff_d) - A)/B)}} \qquad [8],$$

which can then be used to compute the flux using equation [6].

<u>Twin point sources used to test the resolution of a microelectrode.</u>

To establish the resolution of a measurement system and distinguish between point sources one can create multiple sources at fixed distances and use a grid pattern of unit measurements to illustrate their pattern either with contour plots or vector plots, Fig 1C. For a specific example that demonstrates measuring the limits of resolution of a probe system see Somieski and Nagel (2001).

Studying compound sources.

In order to simultaneously study a source that is transporting multiple compounds, it is necessary to be able to model the multiple sources and develop a protocol to measure the separate compounds effectively. We present here an example of a compound flux measurement that illustrates the solution of a problem that could arise with any paired measurement, interference between the two electrodes.

Measuring proton flux and oxygen flux simultaneously presents such a potential problem. The standard polarographic oxygen electrode (Fig 2B) applies a steady voltage to its exposed platinum tip in order to make its surface bind oxygen reversibly depending on the local oxygen level. Will this applied voltage on the oxygen electrode interfere with an adjacent rigidly related proton ion-specific electrode (Figs 3, 4A) attempting to measure pH in the same vicinity? We examined this possibility by systematically measuring the oxygen electrode current as well as the proton electrode voltage with the two microelectrodes held at different distances from one another. It is clear, Fig. 5, that the oxygen electrode current is independent of the proton electrode but the proton electrode is affected dramatically by being less than 40 microns from the oxygen electrode tip.

Using a specifically tailored SIET sampling rule (Table II) we were able to maintain a 40 μm distance between the two microelectrodes and sample an artificial source of

protons and sink of oxygen to obtain two simultaneous measures of proton and oxygen flux (Fig. 4B-D). In that demonstration, Fig. 4B, the two contour patterns on the raw data appear to be offset from one another due to the fixed distance between the two microelectrodes. By using the distance adjustments implied in sampling rule which sequentially steps the two microelectrodes to a common location while maintaining their physical distance (> 35 μm apart) we are able to measure the oxygen and proton flux about an artificial source (Fig. 4) and the pattern of currents can be shown to be concentric when the probe separation is corrected in the position data. We subsequently applied this pairing of microelectrodes and sampling rule to a growing pollen tube tip (Fig. 6), which demonstrates the similar distribution of proton secretion and oxygen utilization in the region posterior to the growing tip which is known to be rich in mitochondria. We recommend studying model sources for the molecules involved whenever multiple probes will be used.

Different plant systems investigated

The scanning ion-selective microelectrode has been extensively used in a number of systems, from brown algae to higher plants, multi or unicellular systems but its use in single or isolated plant cells is of particular importance since the currents generated are generally smaller in magnitude and therefore more difficult to detect. This technique has allowed considerable advances in understanding some of these systems and therefore, we will focus on results obtained in single or isolated cells like pollen tubes (Fig 7C-E; Fig.8A), root hairs (Fig 8D-F) and higher plant fertilization, studied through an *in vitro fusion* system in maize (Fig 9).

Pollen tubes

The largest body of data acquired with extra-cellular, non-invasive techniques in single cells of higher plants was obtained from the studies focusing on pollen tube growth. Pollen tubes are one of the most remarkable examples of polarized growth in nature. Since the early developments of the vibrating probe, this cellular model has been thoroughly studied and the results confirm the outstanding robustness of this type of cell growth and illustrate beautifully the advantages of the technique.

Pollen tubes were first utilized by Weisenseel *et al.* (1975) to demonstrate the use of the vibrating voltage probe. He used germination media of ionic simplicity and low salt concentration, yielding a high signal-to-noise ratio. Under these conditions they were able to demonstrate the existence of large electrical currents traversing pollen tubes, with the grain acting as the source of current and the tube as the sink. In parallel, the same group showed a common pattern in fucoid eggs which also undergo tip growth and were already known to drive electrical currents through themselves (Jaffe, 1966; Jaffe, 1968). This similarity, albeit huge physiological and genetic differences, suggested a causal and general role for electrical currents in initiating and maintaining tip growth.

Their observations might have been tainted by the fact that the microelectrode vibration can affect the gradients that it is recording. The vibration frequency of the vibrating voltage microelectrode (200 cycles per second) was one of the major problems addressed in this study. To obviate the movement that the cells would undergo due to stirring created by microelectrode vibration, these initial recordings were done using a cellophane membrane to immobilize the cells, which would otherwise be freely floating in the liquid germination media and impossible to track. This cellophane membrane does not create an electrical barrier and the recording is therefore not affected by it, however the added distance due to the thickness of the

cellophane at which the recording is being done and the probe path through which the measurement is made does not match the geometry of the actual cell, creating an apparent deformation in the electrical field measured around the cell.

Despite the artefacts that this initial system might have had, the observation that the steady currents formed a dipole in growing pollen tubes and that this was common to other cell types sharing a tip growth mechanism was a conceptually important step towards understanding the importance of electrical currents in such growing systems. The determination of a current source and sink lead to the idea that in the developmental process of pollen tubes, the membrane tends to differentiate into discrete states, forming domains, one of which is an ion-leaky state in the sink region and the other is an ion-pumping domain in the source region. Also, they speculated that an electrical current would therefore traverse pollen tubes, creating a loop, and that this could generate a movement of isolated cellular constituents that could be pulled forward by the current, since most are small and free enough to move through the cytoskeleton. This concept of membrane domain formation together with the hypothesis of electrophoretic movement were proposed as ways in which electrical currents could have important physiological consequences. The molecules in the cytosol are however buffered by such substantial Brownian motion energy that the actual induction of their translational movement in free solution by the ion current potentials is unlikely. An energetically more likely paradigm is that ion potentials could provide the orientation that provides the direction for actin or tubulin based cytoplasmic motility engines used for navigation. One other conceptually important aspect of this pioneering study was the presence of electrical-currents-predicting the tube germination site. This implied that electrical currents could be the basis of a morphogenetic process like the onset of tip growth. At those early times the currents

were weak at most and argue that they likely mark the spot where an important process is to happen but are less likely to be the motive force. The question of causal roles for currents or the ions they move remains at the centre of ion flux studies.

The vibrating voltage probe did not give any information about the ionic nature of the currents measured. If at all, this could be inferred by changes in the composition of the medium used which can by themselves affect the physiology of the cells. Weisenseel *et al.* (1975), based on the dependence of current on the ionic composition of the medium, suggested that most of the inward current consisted of potassium ions entering the whole pollen tube uniformly. At the growing tip, they speculated that calcium could be part of the current loop. To further examine the ionic nature of the currents, Weisenseel and Jaffe (1976) performed more media ion-substitution experiments. They implicated protons as an important part of the outward current at the grain and potassium as the major component of the inward current at the tube. But the development of a calcium specific ion-selective probe (Kühtreiber and Jaffe, 1990) uncovered an apparent contradiction with these conclusions since a calcium influx was measured at the tip which could, by itself, account for most of the inward current. The accuracy of the results obtained with the ion-selective vibrating probe precluded previous voltage vibrating probe data from being quantitatively correct. The authors analyzed fucoid eggs, pollen, *Dyctiostelium discoideum*, amoebae, *Sarcophaga* follicles and fertilized ascidian eggs. In all of these systems, they detected calcium currents with possible roles in development.

An important constraint of the scanning probe technique is that the microelectrode performs better under low media calcium while not all biological material (e.g. marine) will behave normally under these conditions. Pierson *et al.* (1994) later confirmed calcium influx at the growing tip of pollen tubes and related the extra-

cellular calcium influx to a tip-focused intracellular calcium gradient through the activity of putative membrane channels.

Due to the importance attributed to calcium in signalling, the first few years after the development of vibrating ion-selective microelectrodes were devoted to calcium flux studies.

An important feature of the growth of pollen tubes of most species studied lies in the fact that tip growth is at some point oscillatory. Following Weisenseel and co-workers' (1975) observation that total currents at the tip of growing pollen tubes were pulsatile after achieving a certain tube length, Holdaway-Clarke *et al.* (1997) showed that calcium was a part of this pulsatile component. Calcium influx oscillates, after a certain length of the pollen tube is attained, and this correlates with the growth oscillations, but calcium influx is delayed by 13 sec. relative to the growth pulse and thus is secondary to growth oscillation. The reasoning that allows this inference is based on the strength of the cross-correlation when the phase of the oscillating components are shifted relative to one another (Holdaway-Clarke *et al.*,1997). The authors propose a model in which the cell wall acts as a buffer to which calcium binds before entering the cell. This model was contested by Messerli *et al.* (2000) who propose an alternative model in which changes in turgor pressure would be responsible for the primary control of oscillating tip growth. When testing specifically these two models, by changing the growth medium's ionic composition and recording changes as a function of ion fluxes, Messerli and Robinson (2003) came to the conclusion that modifications in both models are needed.

When measuring ion fluxes and assessing the space and time correlation to growth, it is important to correlate these with the cytosol concentrations of the ion being studied. We have studied the contribution of protons to the tip growth process (Feijó

et al. 1999), and demonstrated a tight correlation between the intracellular distribution pattern and the fluxes across the membrane. The pattern involves an influx of protons at the growing tip corresponding to an acidic domain in the cytosol and an efflux in the region that corresponds to the clear zone and to an intra-cellular constitutive alkaline zone (Fig. 8A).

Messerli *et al.* (1999) reported oscillations in proton, potassium and calcium fluxes at the growing tip, all lagging the growth pulses but failed to detect the efflux region of protons on the clear zone. However the use of substantial amounts of buffer concentration in the medium by these authors (5 mM MES buffer, compared to 0,05 mM MES) is known to affect the measurement of proton gradients in a sufficient manner to mask these effluxes beyond detection (Kunkel et al., 2001). Proton effluxes on the sub-apical area of pollen tubes have since been confirmed in tobacco pollen tubes, correlated with the position of proton-pumping ATPases (Certal et al., submitted).

This later example argues that careful medium design for recording with particular microelectrodes is needed whenever applying ion selective microelectrode measurement systems. Media should be ionically as simple as possible, especially with regard to the ion being measured, in order to reduce noise, increase the signal-to-noise ratio and allow for smaller signals to be adequately recorded. This technique records a specific concentration at each point of the measurement algorithm in the extra-cellular medium. A change in concentration implies a flux. When dealing with protons, it is essential to think about the buffer used and its concentration and to test how this affects the measurement. Ideally, buffer concentrations should be kept as low as possible, so as not to interfere, since buffers will absorb protons and therefore, deflate the extension of concentration gradients (Kunkel et al, 2001).

Messerli *et al.* (1999) acknowledge that buffering has an effect on the measurement and they correct the flux values obtained according to previously determined correction factors (Arif *et al.*, 1995; Demarest and Morgan, 1995). They however do not account for the possibility that this not only affects the magnitude of proton fluxes but it might also alter the extra-cellular gradients such that some fluxes are no longer measurable. Kunkel *et al.* (2001) showed several complications result from using pH buffers in the medium where proton-specific LIX microelectrodes are used. Facilitated diffusion enhances the measured proton flux due to proton equilibration with the buffer. The buffer absorbs local protons, allowing them to escape the source more rapidly than by simple diffusion, enhancing proton fluxes. A major conclusion from this study is to keep the culture media as simple as possible and reduce the buffer components to as low titre as possible. This can be easily monitored by measuring the 3-dimensional components of the flux to ensure the rational consistency of flux vector strength and direction relative to a source or sink.

Zonia *et al.* (2002) subsequently showed, for the first time, that chloride efflux cycles at the growing tip, coupled-to and in-phase with cycles of growth, indicating that chloride dynamics is an important component in the network of events that regulate pollen tube homeostasis and growth. The rest of the tube exhibits chloride influx (fig. 7E). Pharmacological studies revealed a correlation between chloride efflux at the growing tip and growth, and that chloride appeared intimately associated with the control of water flow. Care was taken to avoid affects by the chemicals used in this study on the chloride-selective microelectrodes. Among the chloride channel inhibitors that have an effect on pollen tube growth, only DIDS was used since it was not found to interfere with sensitivity or selectivity of chloride-selective micro-electrodes. Moreover, the authors, upon realization of this unexpected result,

performed the necessary controls to ensure the validity of the chloride flux calculations. Tests were conducted in which the dynamic responses of chloride-selective microelectrodes measuring an artificial chloride flux source were calculated to be 3 orders of magnitude higher than the other anions tested. Knowing that other anions can interfere with the measurement of chloride anions, they calculated chloride concentration in an alternative manner using a colorimetric assay. The results were consistent with those obtained with the chloride-selective microelectrodes.

Messerli *et al.* (2004) argue that the fluxes measured were in fact changes in the concentration of the anionic form of the pH buffer (MES) and not changes in chloride concentration. In this study, the authors characterized the ionophore cocktails previously used by Zonia *et al.* (2002) and claim that the selectivity and possibly interference from other anions and chemicals used for chloride channel blocking would preclude the results previously obtained. But using the buffer concentration that Zonia *et al.* (2002) use, Messerli *et al* (2004) shows only a 3.38% reduction in potential responses to chloride concentration for a background concentration of chloride between 0.1 and 1.0 mM and 9.98% for a background concentration between 1 and 10.0 mM.

This later controversy shows that when dealing with indirect evidence (such as extra-cellular concentration recordings to infer membrane fluxes), care needs be taken to ensure the validity and accuracy of the measurements. In this case, technical controls by Messerli *et al.* (2004) actually confirm the applicability of the technique under the conditions used by Zonia *et al.* (2002). Nevertheless, the controls performed show that each ionophore cocktail used to produce an ion-selective microelectrode can not be applied universally and this example provides a model for the sorts of cautions

that must be observed when testing a new ionophore cocktail or when a medium composition change or pharmacology is designed.

While it is generally agreed that healthy pollen tube growth is linked to coordinated entry of calcium and other ions at the growing tip, the coordination of entry or exit in other regions is less well documented. Best understood is perhaps the proton secretion in the region of the alkaline band that may be associated with the mitochondrial rich zone and functionally related to secretion of protons accumulated in the cytosol from active mitochondrial respiration (Feijo *et al.*, 1999). In addition, inactivation of pollen growth by incompatibility reactions has been linked to calcium entry along the pollen tube shaft (Franklin-Tong et al., 2002). Thus the model of ion fluxes associated with pollen tube growth is broadening.

Root hairs

Root hairs are highly specialized tip growing cells (fig. 8 D). Calcium dynamics were studied using the calcium-selective vibrating probe by Schiefelbein *et al.* (1992). In this study, a calcium influx was detected at the tip of growing root hair cells, but no fluxes at the sides or at the tip of non-growing root hair cells. Nifedipine, a calcium channel blocker, confirmed the link between growth and the calcium flux since its application inhibits both. Later, Felle and Hepler (1997) confirmed this calcium influx by imaging intracellular calcium concentration using a fluorescent dye as validation for this pattern. Imaging of proton secretion by root tips has also been demonstrated using external pH indicators (Jaillard *et al.*, 1996) and this technology promises to allow flux calculations and applicability for studies of more localized cellular phenomenon (Tang *et al.*, 2004).

Nod factors, which are lipochitin-oligosaccharides produced by bacteria in response to flavonoids present around roots, induce many processes associated with root nodule morphogenesis on host plants. Root hairs respond rapidly to these molecules and among the most rapid responses described are those involving changes in membrane potential and ions like calcium, chloride and protons (reviewed by Cardenas *et al.*, 2000). Allen *et al.* (1994) first detected changes in the extra-cellular calcium flux outside the root hairs after exposure to Nod factors using a calcium-selective vibrating probe. Cardenas *et al.* (1999) further determined that these changes occur within the first 5-10 minutes of Nod factor application (fig. 8 E,F). A sharp increase in the calcium influx level (from 12,7±0,7 to 28,4±2,8 pmol.cm^{-2}.s^{-1}) at the tip of root hair cells occurs concomitantly with an increase of the membrane area over which the influx occurs and with an increase in the concentration of the intracellular free ion. One advice produced by this study is to use a protocol that estimates both the intensity and the area of current production since the NOD induced increase of total calcium flux at the root hair tip (fig. 8F) is composed of both an increase in intensity as well as the area over which the flux occurs. In order to accomplish this one needs to either scan the source area close to the cell or do a step-away measurement of the declining signal with distance (fig. 8F). Either of these techniques allows for discrimination between an intense point source (of low current) versus a larger, more active and substantial surface feature and allow a quantitative estimation of total ionic flux.

As for protons, although fluxes have been implicated in root hair growth and Nod factor response, only stationary microelectrodes have been used and the result was apparently contradictory. The pH around the root hair remains acidic, but becomes less so in response to Nod factors. Since intracellular pH increases, this alkalinization

could be expected to correspond to an acidification of the extra-cellular medium so it is not clear why the intra and extra-cellular changes occur in the same direction. Felle *et al.* (1998) justifies this by considering different buffering capabilities of the intra and extra-cellular compartments. Cardenas *et al.* (2000) also argue that, based on data from stationary microelectrodes and scanning proton-selective microelectrodes along the whole root, the complexity of proton regulation is likely to be the result of a system more elaborate than just two compartments with different buffering properties.

Fertilization in higher plants

More recently, the SIET contributed to a major breakthrough in plant development, when a study by Antoine *et al.* (2000) made a direct measurement of an influx of extra-cellular calcium induced by gamete fusion in maize (fig.9). The extra-cellular fluxes measured at the surface of isolated egg cells, with or without adhesion of a male sperm cell were close to zero and stable over time. However, after gamete fusion, a calcium influx was triggered close to the site of sperm entry with a delay of 1.8 ± 0.6 sec (fig. 9A). This influx spread throughout the whole cell, progressing at a rate of 1.13 $\mu m.sec^{-1}$. After this wave front propagation, the calcium influx intensity remained sustained, monotonic and homogeneous over the whole egg cell (average influx of 14.92 $pmol/cm^{-2}/sec^{-1}$ lasting an average of 24.4 min). This characteristic influx, and the necessary channel opening, was shown to be the first embryonic event following and triggered by gamete membrane fusion. The cytological modifications observed after fertilization correlate well with the spread of the calcium influx and the latter changes in cytosolic calcium concentration may work as a trigger and possibly a space and time coordinator of many aspects of egg activation. It was shown that the calcium influx has a determinant contribution, since application of a

calcium ionophore mimics some aspects of egg activation. Furthermore, the nature of the channels involved was assessed with the use of gadolinium, which inhibited the influx, possibly implicating mechano-sensitive channels. In all species studied, gamete fusion triggers an increase in cytosolic calcium concentration. This is accepted as part of the initial steps to egg activation but the source and regulation of this calcium signal and the way it is transduced inside the zygote are controversial. It was already known that after gamete fusion there was a rise in cytosolic calcium (Digonnet *et al.*, 1997), sufficient for egg activation, but the relationship between this and the wave front spread of calcium influx from the fusion site was unknown. Antoine *et al.* (2001) addressed this question by simultaneously recording calcium fluxes and cytosolic calcium concentration, using a setup that combines the SIET and ion-ratiometric widefield imaging. Under these conditions it was possible to discriminate between the contribution of the cytosolic calcium and calcium influx. This unique technical combination allowed for the conclusion that the calcium influx precedes the cytosolic calcium elevation by 40-120 sec, thus implicating the existence of separate mechanisms for both of these calcium arenas (fig. 9B). Further pharmacology and buffer suppression of the cytoplasmic calcium showed that its elevation is essential for egg activation, as measured by the initiation of cell wall deposition. However the extra-cellular influx does not seem to be a necessary condition for egg activation. The inhibition of this influx does, however, prevent the sperm incorporation and consequent karyogamy, showing that both mechanisms should be combined to achieve eventual fertilization. Furthermore, it was shown that a gadolinium-independent calcium influx is always present in the sperm plasma membrane after fusion, which might implicate a second type of calcium channel involved in the early activation steps of zygote formation.

Conclusions

It is clear that the Scanning Ion Selective Technique, SIET, is a powerful tool for cell biological research that has been effectively applied to various plant systems. It is also clear that application of this technique requires a logical and methodical development of confidence in the tool by using model steady state sources on which to test out and calibrate the probes, after which the application to living systems can provide a rich data structure that can lead to breakthroughs in the understanding of cell growth and development.

ACKNOWLEDGEMENTS

JAF lab is supported by FCT grants POCTI/BCI/41725/2001, POCTI/BCI/46453/2002, POCTI/BIA-BCM/60046/2004 and POCTI/BIA-BCM/61270/2004. JGK lab is partially supported by Applicable Electronics Inc.

REFERENCES

Antoine AF, Faure JE, Cordeiro S, Dumas C, Rougier M, Feijo JA. (2000) A calcium influx is triggered and propagates in the zygote as a wavefront during in vitro fertilization of flowering plants. *Proc Natl Acad Sci U S A*. **97**:10643-8

Antoine AF, Faure JE, Dumas C, Feijo JA. (2001) Differential contribution of cytoplasmic Ca2+ and Ca2+ influx to gamete fusion and egg activation in maize. *Nature Cell Biol*. **3**:1120-3

Blatt, M. (ed.) (2004) Membrane transport in Plants. Ann.Plant Rev., vol.15, Blackwell, London, UK

Cardenas L, Holdaway-Clarke TL, Sanchez F, Quinto C, Feijo JA, Kunkel JG, Hepler PK. (2000) Ion changes in legume root hairs responding to Nod factors. *Plant Physiol*. **123**:443-52

Cardenas L, Feijo JA, Kunkel JG, Sanchez F, Holdaway-Clarke T, Hepler PK, Quinto C. (1999) Rhizobium nod factors induce increases in intracellular free calcium and extracellular calcium influxes in bean root hairs. *Plant J*. **19**:347-52

Digonnet C, Aldon D, Ledue N, Dumas C and Rougier M (1997) First evidence of a calcium transient in flowering plants at fertilization. *Development*, **124**: 2867-2874

Faszewski EE and Kunkel JG. (2001) Covariance of ion flux measurements allows new interpretation of *Xenopus laevis* oocyte physiology. J Exp Zool **290**:652-61

Feijó JA, Sainhas J, Hackett GR, Kunkel JG, Hepler PK. (1999) Growing pollen tubes possess a constitutive alkaline band in the clear zone and a growth-dependent acidic tip. *J Cell Biol*. **144**:483-96

Feijó, JA, Sainhas, J., Holdaway-Clarke, T, Cordeiro, MS, Kunkel, JG, and Hepler, PK. (2001) Cellular oscillations and the regulation of growth: the pollen tube paradigm. Bioessays 23, 86-94.

Feijó JA, Costa SS, Prado AM, Becker JD, Certal AC. (2004) Signalling by tips. *Curr. Opin Plant Biol*. **7**:589-98

Felle HH, Hepler PK. (1997) The Cytosolic Ca^{2+} Concentration Gradient of *Sinapis alba* Root Hairs as Revealed by Ca^{2+}-Selective Microelectrode Tests and Fura-Dextran Ratio Imaging. *Plant Physiol.* **114**:39-45

Franklin-Tong VE, Holdaway-Clarke TL, Straatman KR, Kunkel JG, Hepler PK. (2002) Involvement of extracellular calcium influx in the self-incompatibility response of *Papaver rhoeas*. *Plant J*. **29**:333-45

Holdaway-Clarke TL, Feijo JA, Hackett GR, Kunkel JG, Hepler PK. (1997) Pollen Tube Growth and the Intracellular Cytosolic Calcium Gradient Oscillate in Phase while Extracellular Calcium Influx Is Delayed. *Plant Cell*. **9**:1999-2010

Holdaway-Clarke TL, Weddle NM, Kim S, Robi A, Parris C, Kunkel JG, Hepler PK. (2003) Effect of extracellular calcium, pH and borate on growth oscillations in Lilium formosanum pollen tubes. *J. Exp Bot.* **54**:65-72

Holdaway-Clarke, T.L., and Hepler, P.K. (2003). Control of pollen tube growth: role of ion gradients and fluxes. New Phytologist **159**:539-563.

Jaffe, LF (1966) Electrical Currents through the Developing Fucus Egg. *PNAS* **56**: 1102-1109.

Jaffe, LF (1968) Localization in the developing Fucus egg and the general role of localizing currents. *Adv Morphog.* **7**:295-328.

Jaffe, L. F. and Levy, S. (1987). Calcium gradients measured with a vibrating calcium-selective electrode. Proc. IEEE/EMBS Conference 9: 779-781.

Jaillard B, Ruiz L, Arvieu, JC. (1996) pH mapping in transparent gel using color indicator videodensitometry. Plant Soil **183**:1–11.

Kühtreiber WM, Jaffe LF (1990) Detection of extra-cellular calcium gradients with a calcium-specific vibrating electrode. J Cell Biol 110:1565-1573

Kunkel JG, Lin L-Y, Xu Y, Prado AMM, Feijó JA, Hwang PP, and Hepler PK. (2001). The strategic use of Good buffers to measure proton gradients about growing pollen tubes. In "Cell Biology of Plant and Fungal Tip Growth" (A. Geitman, Ed.), pp. 14pp. IOS Press, Amsterdam.

Lin L-Y, Horng J-L, Kunkel JG and Hwang P-P. (2005) Proton pump-rich cell is secreting acid in skin of zebrafish larvae (*Danio rerio*). AJP-Cell Phys. (in press).

Pina C, Pinto F, Feijó JA, Becker JD (2005) Gene family analysis of the Arabidopsis pollen transcriptome reveals novel biological implications for cell growth and division control and gene expression regulation. *Plant Physiology* **138**: 744–756

Prado AM, Porterfield DM, Feijo JA. (2004) Nitric oxide is involved in growth regulation and re-orientation of pollen tubes. *Development*. **131**:2707-14

Roy SJ, Holdaway-Clarke TL, Hackett GR, Kunkel JG, Lord EM, Hepler PK. (1999) Uncoupling secretion and tip growth in lily pollen tubes: evidence for the role of calcium in exocytosis. *Plant J*. **19**:379-86

Sanders, D., Bethke, P. (2000) Membrane Transport. In Buchanan, B et al. (eds.) Biochemistry and Molecular Biology of Plants. ASPB, Rockville, Maryland, US

Schiefelbein JW, Shipley AM, and Rowse P. (1992) Calcium influx at the tip of growing root-hair cells of *Arabidopsis thaliana*. *Planta* **187:**455-459

Schneiderman G and TK Goldstick. (1978) Oxygen electrode design criteria and performance characteristics: recessed cathode. *J Appl Physiol* 45: 145-154.

Shipley AM and Feijó JA (1999) The use of the vibrating probe technique to study steady extracellular currents during pollen germination and tube growth. In M.Cresti, G.Cai and S.Moscatelli (eds.) "Fertilization in Higher Plants: Molecular and Cytological Aspects". Springer-Verlag. Heidelberg, Berlin. pp.235.252

Taiz, L., Zeiger, E. (2002) Plant Physiology. Sinauer, Sunderland, MA, USA, pp.87-108

Tang C, Drevon JJ, Jaillard B, Souche G, Hinsinger P. (2004) Proton release of two genotypes of bean (*Phaseolus vulgaris* L.) as affected by N nutrition and P deficiency. Plant and Soil **260**: 59–68.

Vissenberg K, Feijo JA, Weisenseel MH, Verbelen JP. (2001) Ion fluxes, auxin and the induction of elongation growth in *Nicotiana tabacum* cells. *J Exp Bot*., **52**:2161-7

Zonia, L., S.Cordeiro and J.A. Feijó (2001) Ion dynamics and the control of hydrodynamics in the regulation of pollen tube growth. *Sexual Plant Reproduction* **14**(1-2):111-116

Zonia L, Cordeiro S, Tupy J, Feijo JA. (2002) Oscillatory chloride efflux at the pollen tube apex has a role in growth and cell volume regulation and is targeted by inositol 3,4,5,6-tetrakisphosphate. *Plant Cell* **14**:2233-49

Legends:

Figure 1. Point source in theory and practice. **(A)** The computed pattern of oxygen diffusing into a capillary tube with a recessed platinum surface which is serving as an oxygen sink. **(B)** Stereo image pair of calcium flux vectors eminating from a point source. **(C)** Stereo image pair of proton flux vectors eminating from a pair of point sources 1.5 mm separated. **(D)** Dynamically measured microvolt differences (ΔμV) measured at graded radial distances from a point source. The expected ΔμV was computed by extrapolation between known linear Voltage vs 1/r points and multiplied by a guess of the dynamic efficiency to attempt to fit a red line of expected-ΔμV to the observed-ΔμV (blue x) . The guessed efficiency was adjusted to give a best fit (red line). **(E)** Contour plot of the dX, dY and dZ components of fluxes of protons eminating from a point source measured at an YZ plane about 10 microns from the tip source. **(F)** Linear plots of the dY data from (E) plotted against the Y location. **(G)** Observed Flux (blue x) computed from the dynamic efficiency and observed ΔμV from (D). Upper and lower 95% confidence intervals (black dashed lines) on the expected J (red diamonds) are computed from the variance of the observed about the expected-ΔμV from (D).

Figure 2. H^+ and O_2 probes calibrations and sampling rules. **(A)** Construction and static calibration of a H^+ probe. Media composition for calibration was the same as pollen culture media except the pH was adjust to various values by adding either KOH or HCl. **(B)** Construction and calibration of an oxygen probe. The same media was bubbled with N_2 for over 30 min to achieve 0 μM oxygen concentration, while bubbled with air (18% O_2) for 30 min assumed to be 100% saturated (268μM). **(C)** Sampling rules that control the movements of both H^+ and O_2 probes. At each measurement point in "Physical Space", both probes will make measurements from (1) → (2) → (3) → (4) → (1) in "Chemical Space".

Figure 3. Schematic diagram of multiprobe setup. H^+ and O_2 selective probes are plugged into pre-amplifiers (one a SIET and one polarographic). Both probes are mounted on a common 3D Micromanipulator (1st 3D), by a motion controller. The pollen tube in its culture dish are held on a motion controlled stage held by a 2nd 3D

Micro-manipulator (2nd 3D) controlled by a 2nd motion controller which allows the rapidly growing tip to be maintained in the center of the stage. The probe amplifiers, two motion controllers and the camera are adjusted and controled by the computer program ASET. A small drop of concentrated germinating pollen was spread evenly on the bottom of the petri dish, which was coated with 10% poly-lysine. The 3 ml of liquid culture medium is added or changed in the petri dish by gravity addition and maintained at a constant level by a suction skimmer.

Figure 4. No interference between H^+/O_2 probes using Sampling Rule with probes 40 μm apart. (A) Artificial dual source. A micropipette filled with CO_2 acts simultaneously as a H^+ source and O_2 sink. **(B)** Contour plot of micro-volts differences and pico-amps differences obtained from H^+ and O_2 probe readings respectively. **(C)** total *μV-difference* $=(\Delta\mu V_x^2 + \Delta\mu V_y^2 + \Delta\mu V_z^2)^{1/2}$ obtained from H^+ probe. **(D)** total *μA-difference* $= (\Delta\mu A_x^2 + \Delta\mu A_y^2 + \Delta\mu A_z^2)^{1/2}$ obtained from the O_2 probe. In both (C) and (D), the total *μV-difference or μA-difference* were plotted onto the coordinate space of the probes reference position correcting for the 40 μm separation. In (B) the contours are drawn with respect to the probes physical positions showing the 40 μm separation.

Figure 5. Interferences between H^+ and O_2 probes. The two probes were manually adjusted to be separated by different distances while readings from both probes were collected. The media was the same as lily pollen culture media at pH 5.5, 100% air saturated. Dotted line indicates the recomended distance to avoid interference.

Figure 6. H^+ efflux and O_2 influx in Z-axis plane over alkaline band region. Pollen tubes 800-2,500μm in length were selected for measurements. H^+/O_2 fluxes, as $\Delta\mu V_z$ and $\Delta\mu A_z$, at the surface of a pollen tube were measured by moving the electrode to within 2μm from the tube surface. Background references were taken at least 500μm away from any pollen grains or tubes and the value was subtracted from the surface measurements. The inset image is a screen shot showing the H^+/O_2 probes and a growing pollen tube with growth rate of 14.634μm per min. This figure is a typical plot of 5 independent experiments.

Figure 7. (A-B) Ion-selective vibrating microelectrode recording of fluxes at the surface of an egg cell of maize before fusion (male gamete at the top right side). The microelectrode moves ("vibrates") between two positions, one away from the cell (A) and one close to the cell (B) repetatively and the delta V values are recorded. All microelectrode measurements are referred to an AgAGCl type reference electrode in the bath located far away (tens of millimetres) from the specimen.
(C-D) Vibrating Ion-selective microelectrode recording fluxes at the germinated pollen grain (C) and at the sub-apical flank of a growing pollen tube (D) of *Lilium longiflorum*. The ion-selective microelectrode positioning and repetitive movement is accomplished by a computer-controlled three dimensional micro-stepping motor translation assembly providing sub-micrometer spatial resolution.
(E) Chloride flux profile along a growing pollen tube of *Lilium longiflorum* between 200 and 400 _m long. The arrows in the scheme indicate the location of the measurements at the cell surface and correspond to the plot below. Positions 1 and 2 correspond to the apical domain and clear zone and 3 and 4 to the tube flank closer to the pollen grain.

Figure 8. (A) Extra-cellular proton flux profile on a growing pollen tube. The efflux region roughly corresponds to the domain occupied by the clear zone. A close correlation is observable between the cytosolic alkaline band (data not shown) and the patterns of proton efflux, suggesting that the elevation of pHc in the clear zone may correspond (at least partly) to an active proton efflux in the
same area (Adapted from Feijó et al., J.Cell Biol. 144: 483–496, 1999, with permission from The Rockefeller University Press).

(B-C) Measurement of H^+-fluxes around elongating BY-2 tobacco cells. (D) Young cell at the start of elongation together with its pattern of proton fluxes, where the length of the arrows (scaled as indicated on the figure) is representative of the magnitude of the flux. (E) Older, well-elongated cell together with its pattern of proton fluxes. Bar=50 µm (Adapted from Vissenberg et al., J.Exp.Bot. 52:2161-2167, 2001, with permission from the Society for Experimental Biology).

D- Measurement of ion fluxes in root hairs of *Arabidopsis* (in this case a *tip-1* mutant plant)

(E-F) Extra-cellular Ca^{2+} fluxes in *P. vulgaris* root hairs responding to Nod factors. (B) Bar graph of Nearest Approach measurements at approximately 1 _m from the root hair apical surface. Control root hair cells exposed to chitin-oligomers (structurally similar to Nod factors but biologically inactive) for 5 minutes had an average Ca^{2+} influx at 1 _m from the tip of approximately 13 pmol cm^{-2} s^{-1} (n = 9). Hairs exposed to Nod factors for 5 minutes on average had a higher Ca^{2+} influx of approximately 28 pmol cm^{-2} s^{-1} 1 _m from the tip (n = 18). Error bars are ± standard error of the mean. (C) Estimation of the Ca^{2+} sink area at the tip of *P. vulgaris* root hairs responding to Nod factors. The graph shows step away measurements of Ca^{2+} influx in the X direction, J_x (in pmol cm^{-2} s^{-1}) at distances x, from the root hair tip in a control hair exposed to the inactive chitin-oligomer (filled squares) and two hairs treated with Nod factors (hollow squares and circles). Lines are theoretical plots obtained with the values shown in tabular form of parameters corresponding to (a), the radius (m) of the Ca^{2+} sink at the tip and (Jo) the flux of Ca^{2+} at the tip surface (i.e. when x = 0). The best fit was obtained by iteration; minimizing a chi-square statistic while changing the influx, Jo (pmol cm2 s1), and radius (a) parameters individually. In the control root hair (measured in the presence of the chitin-oligomer), the best fit was obtained with a radius of 2.01 m (dotted line), while in the two examples responding to the Nod factors, the best fit corresponded to a sink radius of 3.93 and 5.66 m, respectively. We made measurements at five step away positions for each root hair. Filled arrowheads indicate average influx values 1 _m from the tip of root hairs treated with either inactive chitin-oligomers or Nod fractors, as shown in (a), number of cells measured shown in parentheses (Adapted from Cárdenas et al., Plant J. 19:347-52, 1999, with permission from Blackwell Science Ltd.).

Figure 9. (A) Ca^{2+} flux measurements during maize IVF. A typical recording is shown (n = 61) illustrating the onset of a Ca^{2+} influx after fusion. Time 0 is chosen arbitrarily as the time of gametic fusion, as asserted by direct microscopic observation. The arrow shows the detectable onset of a Ca^{2+} influx after fusion. A clear Ca^{2+} influx was always detected in the egg membrane, with a delay to fusion dependence on the relative position of the probe and fusion site (black arrow in the plot). 1, 2, 3, and 4 refer to the time when the pictures (Bottom) were taken. The following events are depicted: (1) egg cell before fusion (male gamete position is

shown by a white arrow); (2) egg cell after fusion, just when contraction has started; (3) strong egg cell contraction; and (4) egg cell reshaping (Adapted from Antoine et al., PNAS 97:10643-10648, 2000, with permission from the National Academy of Sciences).

(B) Simultaneous measurement of Ca^{2+} flux and $[Ca^{2+}]_{Cyt}$ during maize IVF. (1) typical experiment (n = 7). Time zero is set at the time when gametes have adhered (vertical line). Fusion is followed by the onset of a Ca^{2+} influx (blue line; average Ca^{2+} influx of -1.19 ± 0.01 pmol cm^{-2} s^{-1}) and by a transient increase in $[Ca^{2+}]_{Cyt}$ (red line). In this particular experiment the onset of the rise in $[Ca^{2+}]_{Cyt}$ occurs when the influx stabilizes close to the maximum (arrow), and the peak $[Ca^{2+}]_{Cyt}$ is coincident with the peak of influx (double arrow). Nevertheless, this is not the rule for all the experiments; usually these two features behave without any visible correlation. BPL, basal pre-fertilization level. (2) Sequence of typical raw images from which the line in 1 was computed. The first image shows sperm_egg cell adhesion (arrowhead). The sperm becomes visible after fusion because of Fluo-3 diffusion into it (arrowheads). Traces in 1 were computed by averaging the total egg-cell or zygote fluorescence as shown in B (_F/F0 = (Ft-F0)/F0). (3) Different cytological events during maize IVF in standard conditions (n > 100). Gametes were isolated from the inbred line A188. a, Gamete adhesion (arrowhead shows the sperm). b, Fusion; the sperm can be seen penetrating the egg cell (arrowhead). c, Mild contraction of the egg cell. d, Reshaping of the cell; the organellar mass has taken a peripheral position, polarizing the zygote. D, Two-photon microscopy section of the vacuolar zone in a typically Fluo3-AM loaded egg _ showing that the vacuole and large organelles are not significantly sequestering the probe. Scale bar in b_d, 20 m.) (Adapted from Antoine et al, Nature Cell Biol. 3:1120-1123, 2001, with permission from Nature Publishing Group).

Table I. Dynamic Calibration of Ion Selective Micro-Electrodes. All dynamic efficiencies were determined using DC methods. Dynamic efficiencies while continuously oscillating (**Step eff%**) were determined using the older 3DVIS software initially written by WielKuhtreiber and modified for 3D measurements by JG Kunkel. Dynamic efficiencies based on sampling rules (**Rule eff%**) were determined using the newer ASET software from ScienceWares. For convenience to the reader we list the technical parameters of each **Ion** listed (Diffusion coefficient at infinite dillution, $\mathbf{D_o}$; valence, i and Nernst slope) as well as the LIX used and its 90% response time. The **Hz** quoted refers to the stepping frequency used in the older 3DVIS software. The bicarbonate diffusion coeficient is listed for the carbonate LIX because at physiological pHs the carbonate travels mainly in the bicarbonate form.

Ion	Do	i	Nernst slope	LIX	t90	Hz	Step eff%	Rule eff%
K^+	19.6	1	58	Fl:K IB	<1s.	0.3	70%	85%
H^+	93.7	1	58	Fl:H IIA	~0.6s	0.3	80%	100%
Ca^{+2}	7.9	2	29	Fl:Ca IIA	<5s	0.3	50%	80%
Mg^{+2}	7.1	2	29	Fl:Mg IV	<30s	0.25	30%	na
Cl^-	20.3	-1	-58	IE: 170	na	0.5	85%	100%
CO_3^{-2}	13.9	-2	-29	IE:310	na	na	na	40%

Table II. A sampling rule for a dual probe system. Point Name: probe position names as shown in Figure 1. e.g. "$H^{+}_{(1)}$" refers to H^{+} probe in location 1; **dX, dY, dZ:** displacements (μm) in X,Y,Z dimensions respectively to get to their correspoinding Point Name; **WaitSec**: defines a waiting time in seconds at the Point Name; **AvgSec**: seconds averaging at 1000 measurements per second. The probe tips were placed 40 μm apart in the Y dimension. The movement to each new location is accomplished in less than 0.1 second and is included in the WaitSec parameter so that the entire time for the dual probe 3-D unit sample to be taken is the sum of WaitSec and Avgsec = 9.2 sec.

Point Name	dX	dY	dZ	WaitSec	AvgSec
$H^{+}_{(1)}$	0	-20	0	0.8	0.5
$O_{2(1)}$	0	20	0	0.5	0.5
$H^{+}_{(2)}$	10	-20	0	0.8	0.5
$O_{2(2)}$	10	20	0	0.5	0.5
$H^{+}_{(3)}$	0	10	0	0.8	0.5
$O_{2(3)}$	0	30	0	0.5	0.5
$H^{+}_{(4)}$	0	-20	10	0.8	0.5
$O_{2(4)}$	0	20	10	0.5	0.5

Figure 1

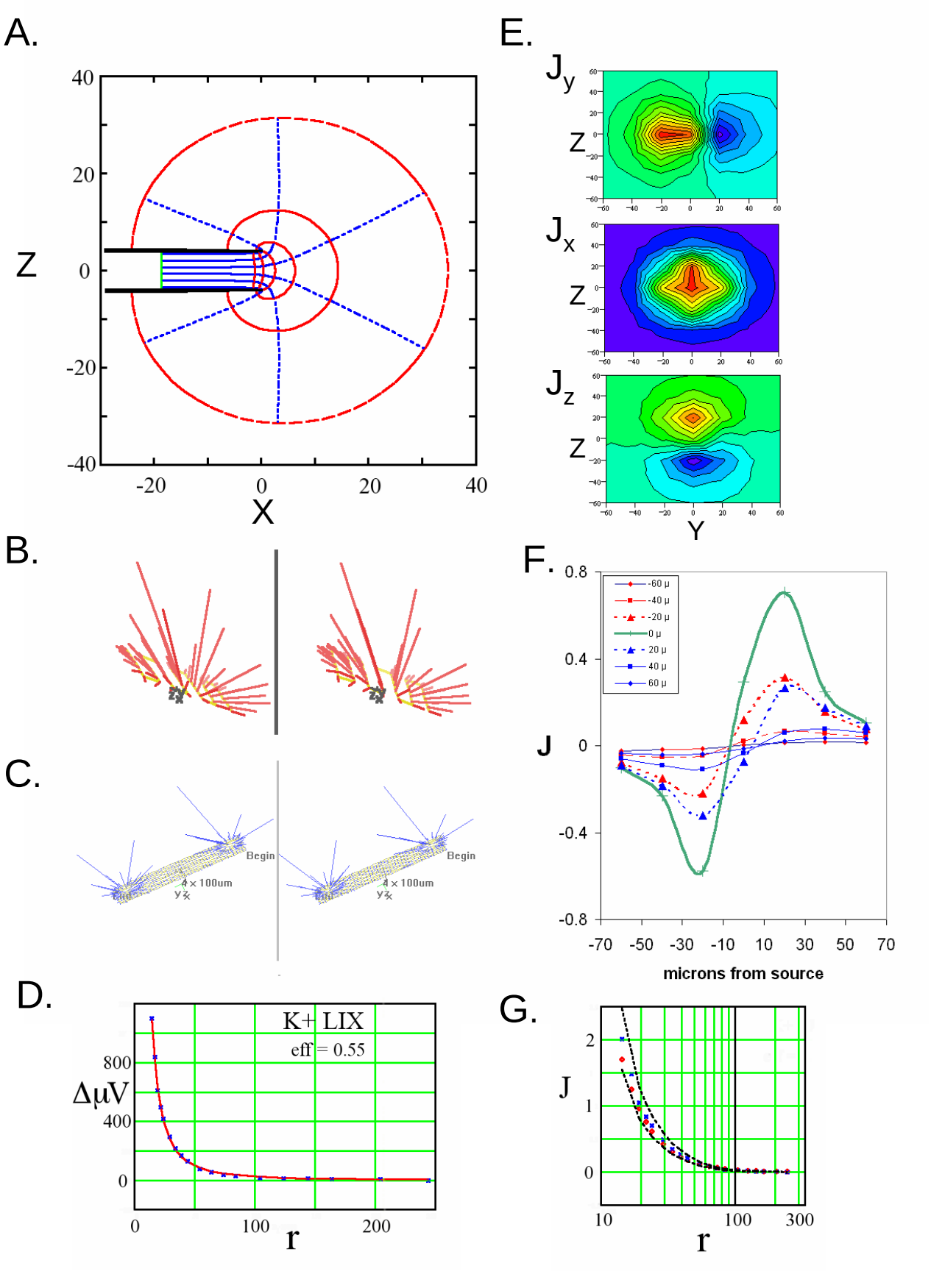
A.
40
20
0
-20
-40
Z
-20
0
20
40
X
E.
J_y
Z
J_x
Z
J_z
Z
Y
B.
C.
Begin
4 × 100um
Begin
4 × 100um
F.
0.8
0.4
0
-0.4
-0.8
J
-60 µ
-40 µ
-20 µ
0 µ
20 µ
40 µ
60 µ
-70 -50 -30 -10 10 30 50 70
microns from source
D.
K+ LIX
eff = 0.55
800
400
0
ΔµV
0
100
200
r
G.
2
1
0
J
10
100
300
r

Figure 2

A.

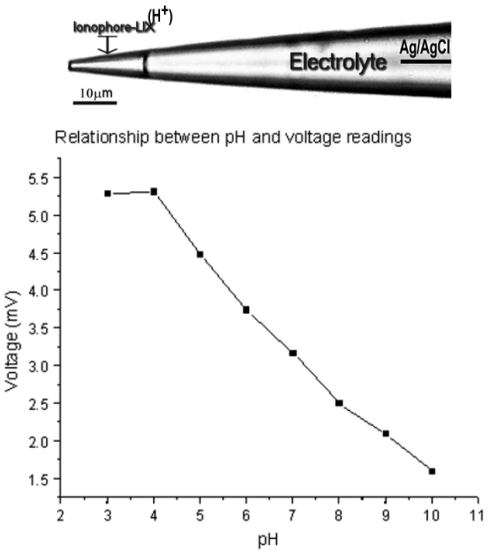
Ionophore-LIX (H+)
Electrolyte
Ag/AgCl
10µm
Relationship between pH and voltage readings
Voltage (mV)
pH

B.

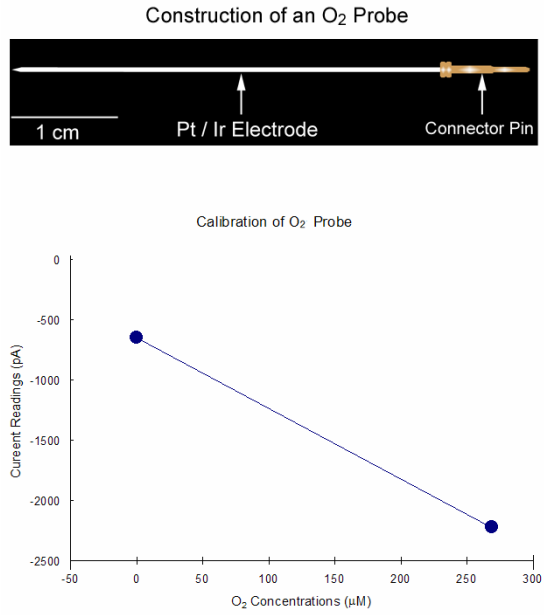
Construction of an O2 Probe
1 cm
Pt / Ir Electrode
Connector Pin
Calibration of O2 Probe
Current Readings (pA)
O2 Concentrations (µM)

C.

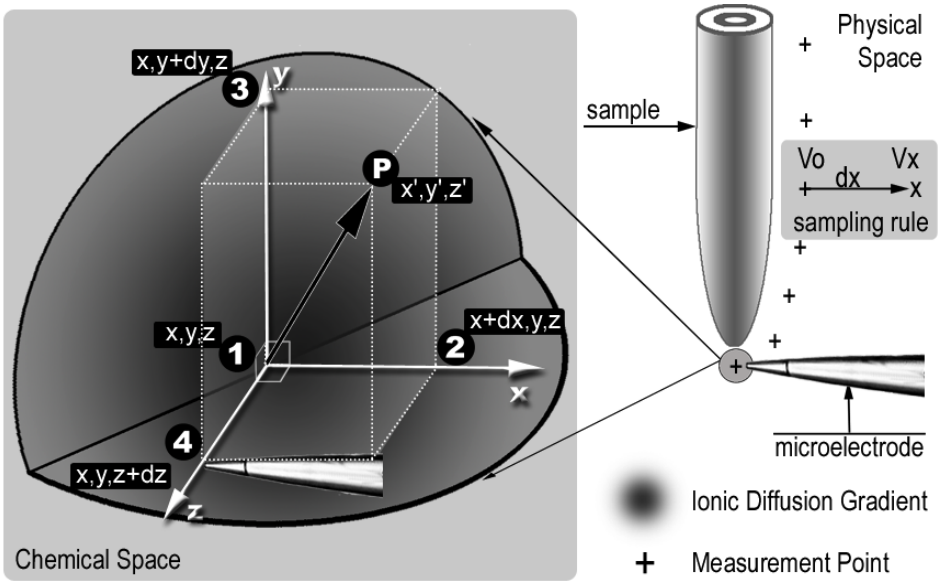
x,y+dy,z
y
P
x',y',z'
x,y,z
x+dx,y,z
x
z
x,y,z+dz
Chemical Space
sample
Physical Space
Vo
dx
Vx
x
sampling rule
microelectrode
Ionic Diffusion Gradient
Measurement Point

Figure 3

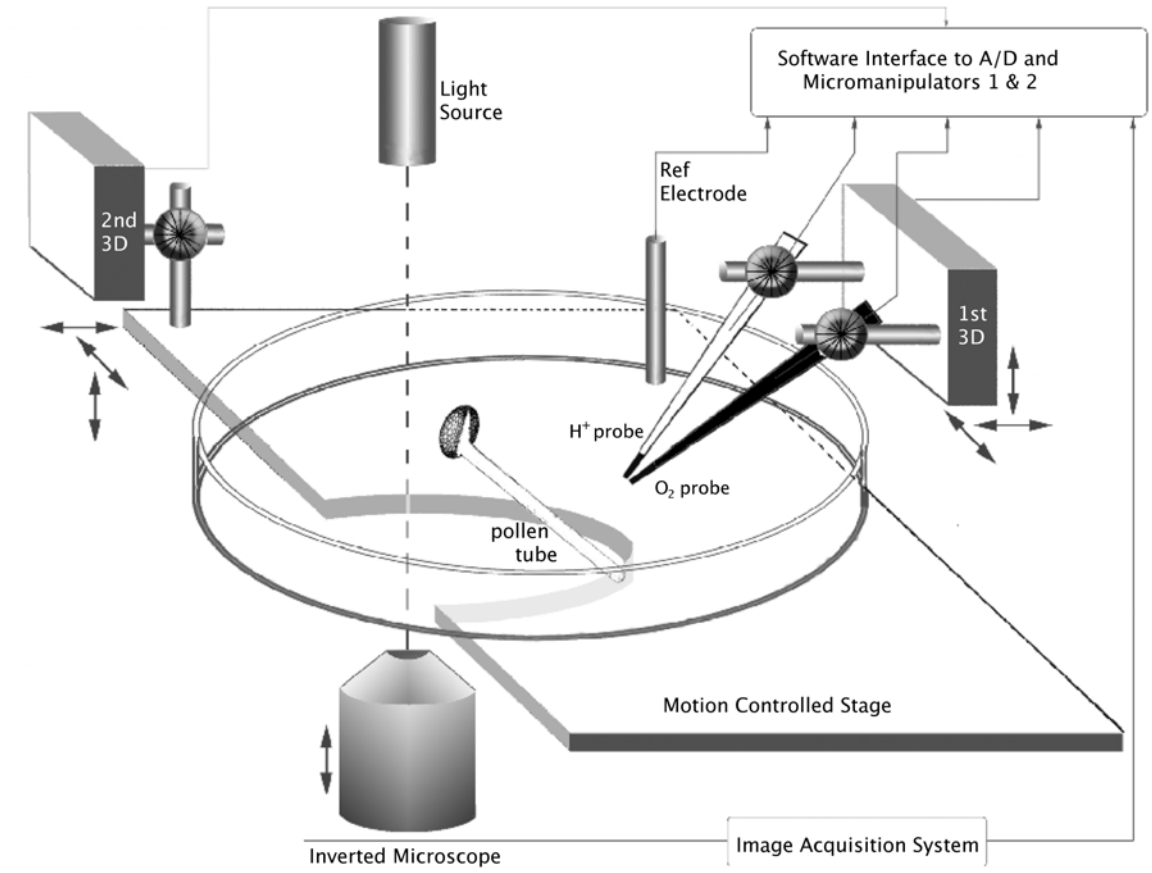
Software Interface to A/D and Micromanipulators 1 & 2
Light Source
Ref Electrode
2nd 3D
1st 3D
H+ probe
O2 probe
pollen tube
Motion Controlled Stage
Inverted Microscope
Image Acquisition System

Figure 4

A.

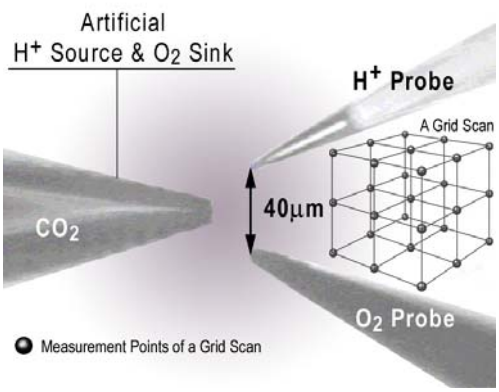

B.

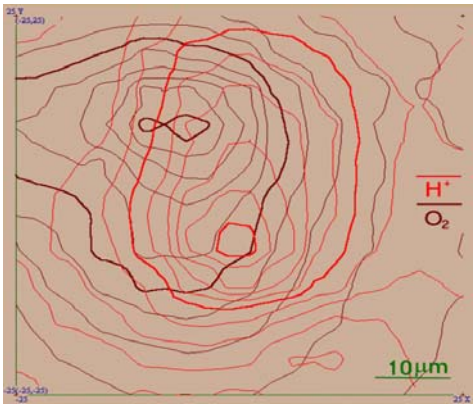

C.

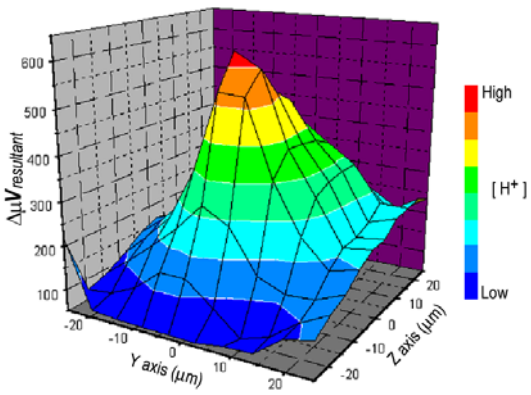

D.

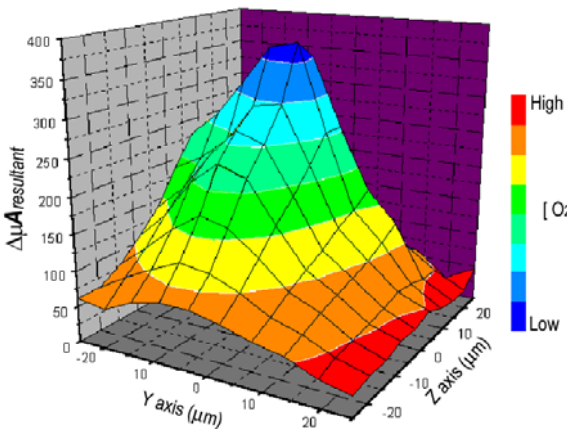

Figure 5

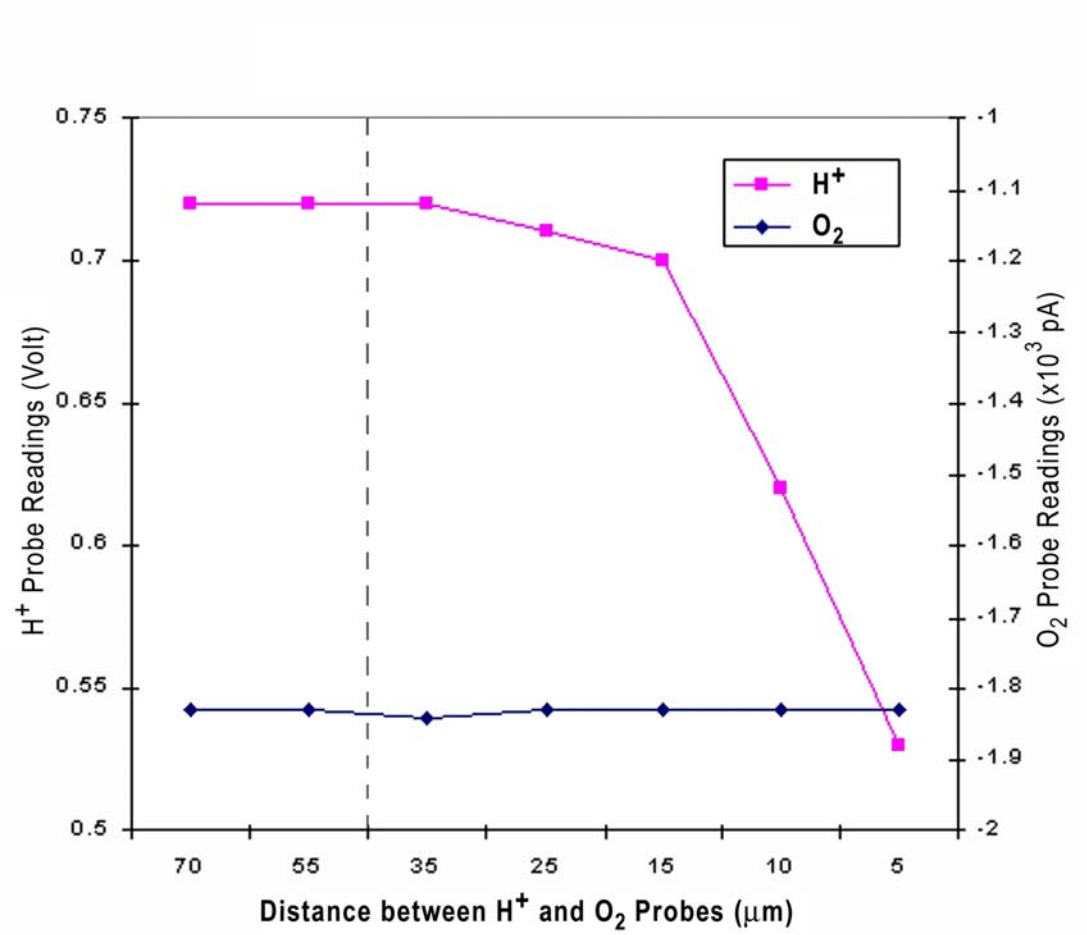
0.75
0.7
0.65
0.6
0.55
0.5
H+ Probe Readings (Volt)
-1
-1.1
-1.2
-1.3
-1.4
-1.5
-1.6
-1.7
-1.8
-1.9
-2
O2 Probe Readings (x10^3 pA)
H+
O2
70
55
35
25
15
10
5
Distance between H+ and O2 Probes (μm)

Figure 6

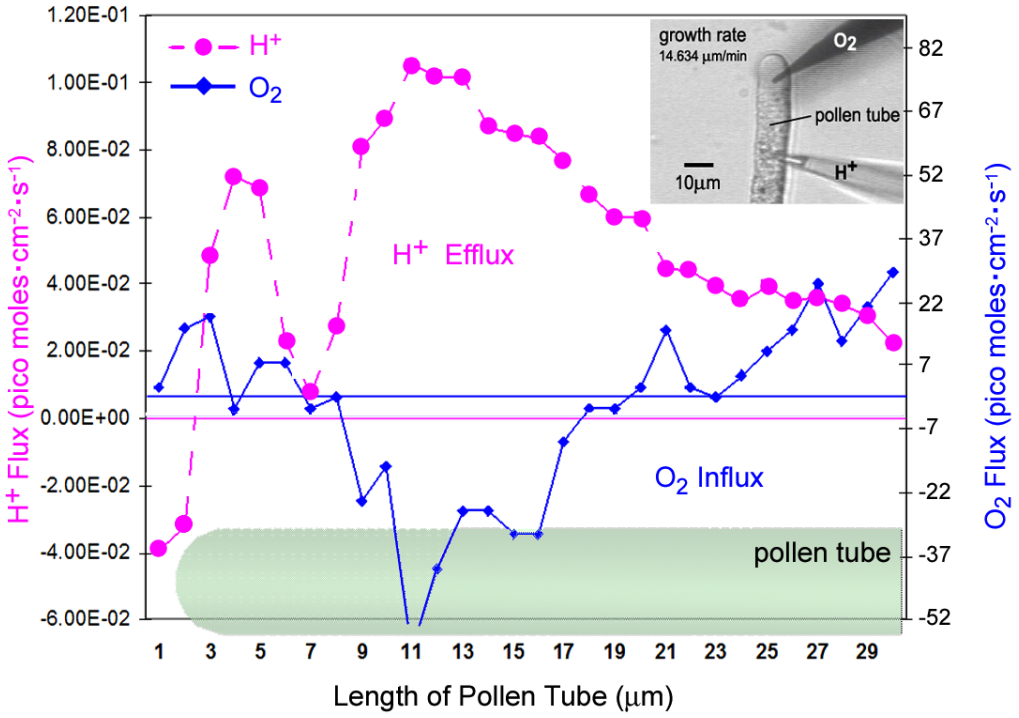
H+
O2
growth rate
14.634 µm/min
O2
pollen tube
H+
10µm
H+ Efflux
O2 Influx
pollen tube
H+ Flux (pico moles·cm-2·s-1)
O2 Flux (pico moles·cm-2·s-1)
Length of Pollen Tube (µm)
1.20E-01
1.00E-01
8.00E-02
6.00E-02
4.00E-02
2.00E-02
0.00E+00
-2.00E-02
-4.00E-02
-6.00E-02
82
67
52
37
22
7
-7
-22
-37
-52
1 3 5 7 9 11 13 15 17 19 21 23 25 27 29

Figure 7

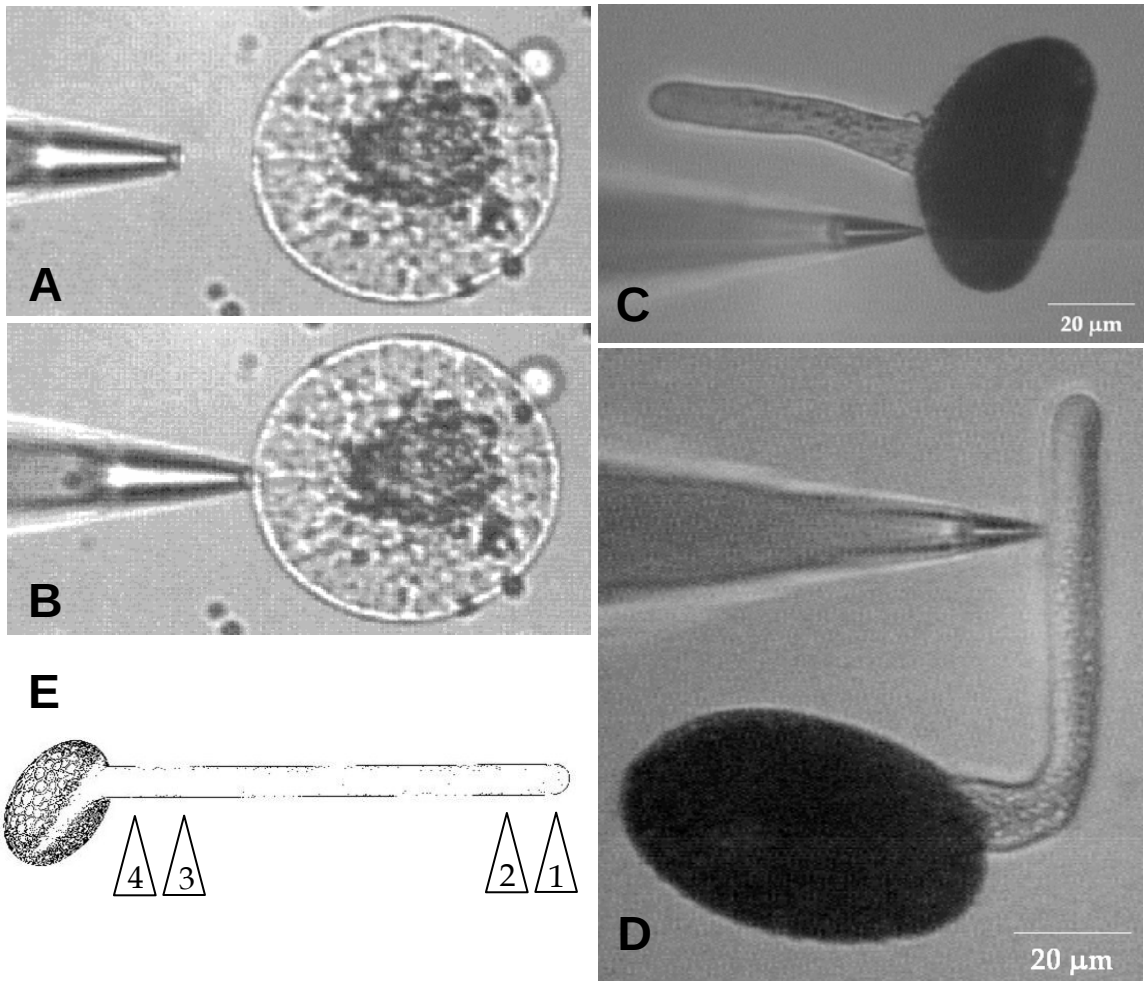
A
B
C
20 µm
D
20 µm
E
4
3
2
1

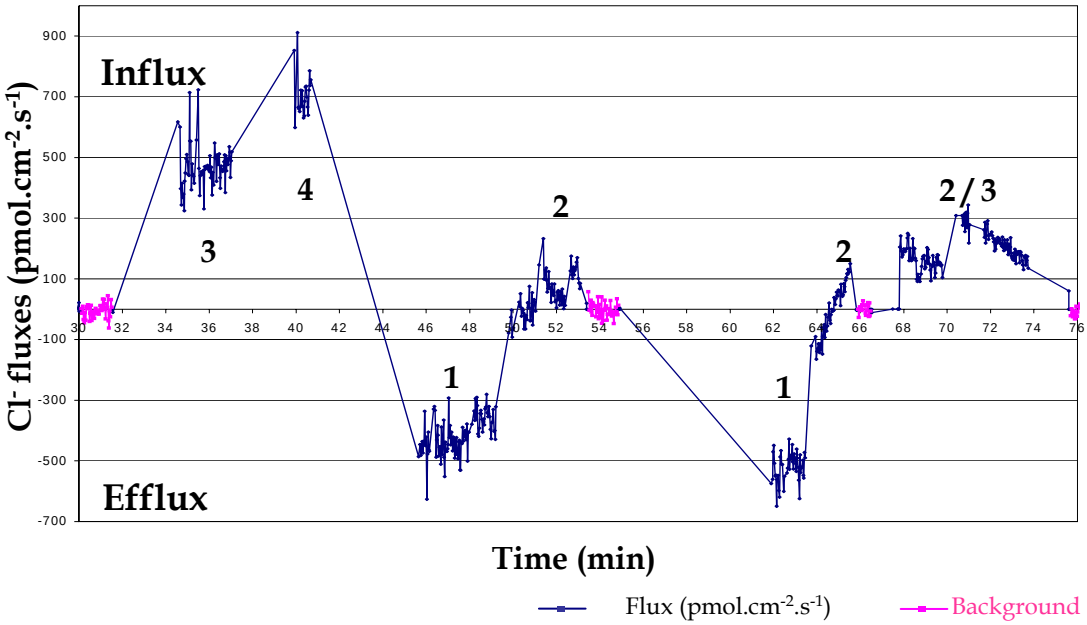
Influx
Efflux
Cl- fluxes (pmol.cm-2.s-1)
Time (min)
Flux (pmol.cm-2.s-1)
Background
4
3
2
1
1
2
2 / 3

Figure 8

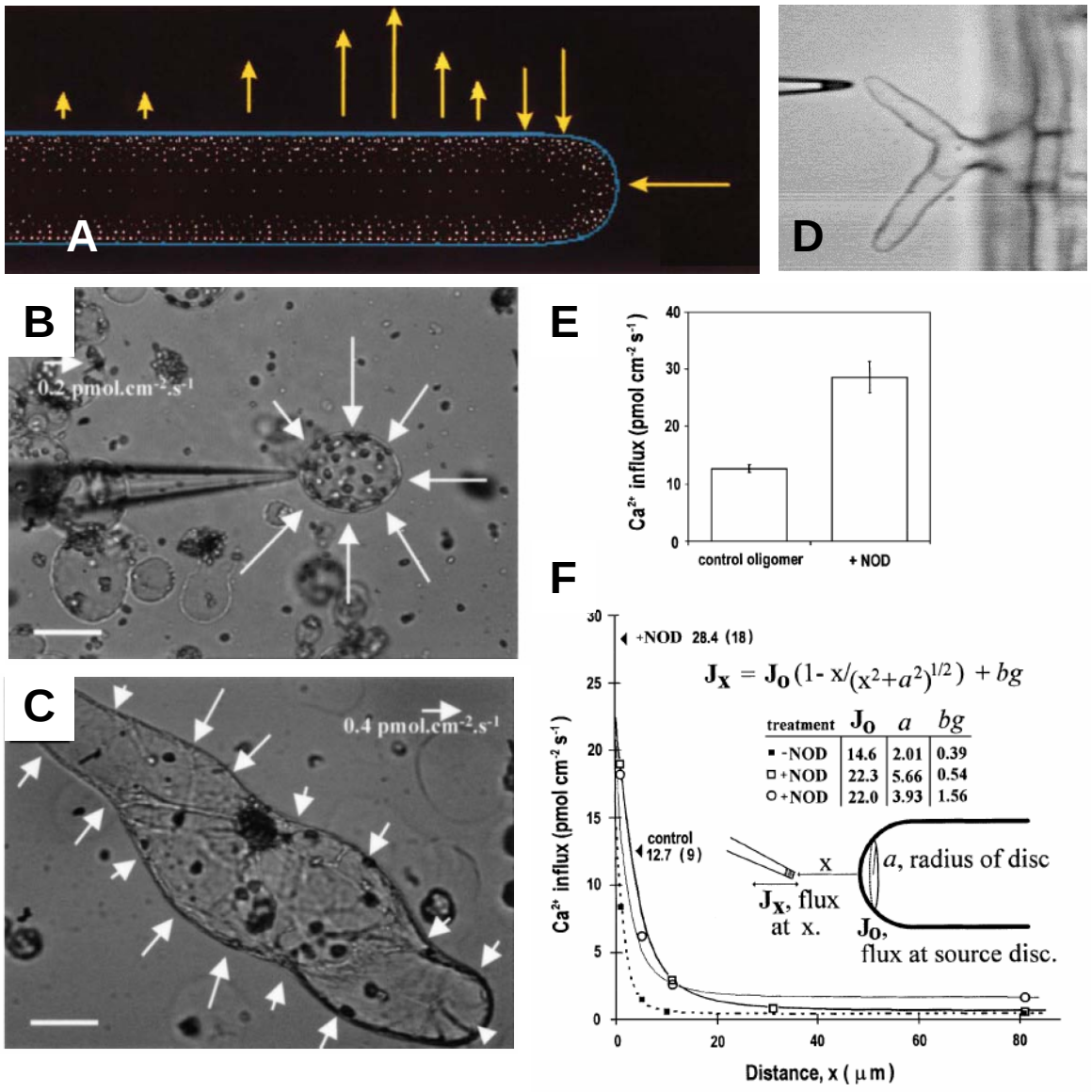
A
D
B
0.2 pmol.cm⁻².s⁻¹
C
0.4 pmol.cm⁻².s⁻¹
E
Ca²⁺ influx (pmol cm⁻² s⁻¹)
control oligomer
+ NOD
F
+NOD 28.4 (18)
$J_X = J_O(1 - x/(x^2+a^2)^{1/2}) + bg$
treatment J_O a bg
-NOD 14.6 2.01 0.39
+NOD 22.3 5.66 0.54
+NOD 22.0 3.93 1.56
control 12.7 (9)
x
a, radius of disc
J_X, flux at x.
J_O, flux at source disc.
Ca²⁺ influx (pmol cm⁻² s⁻¹)
Distance, x (μm)

Figure 9

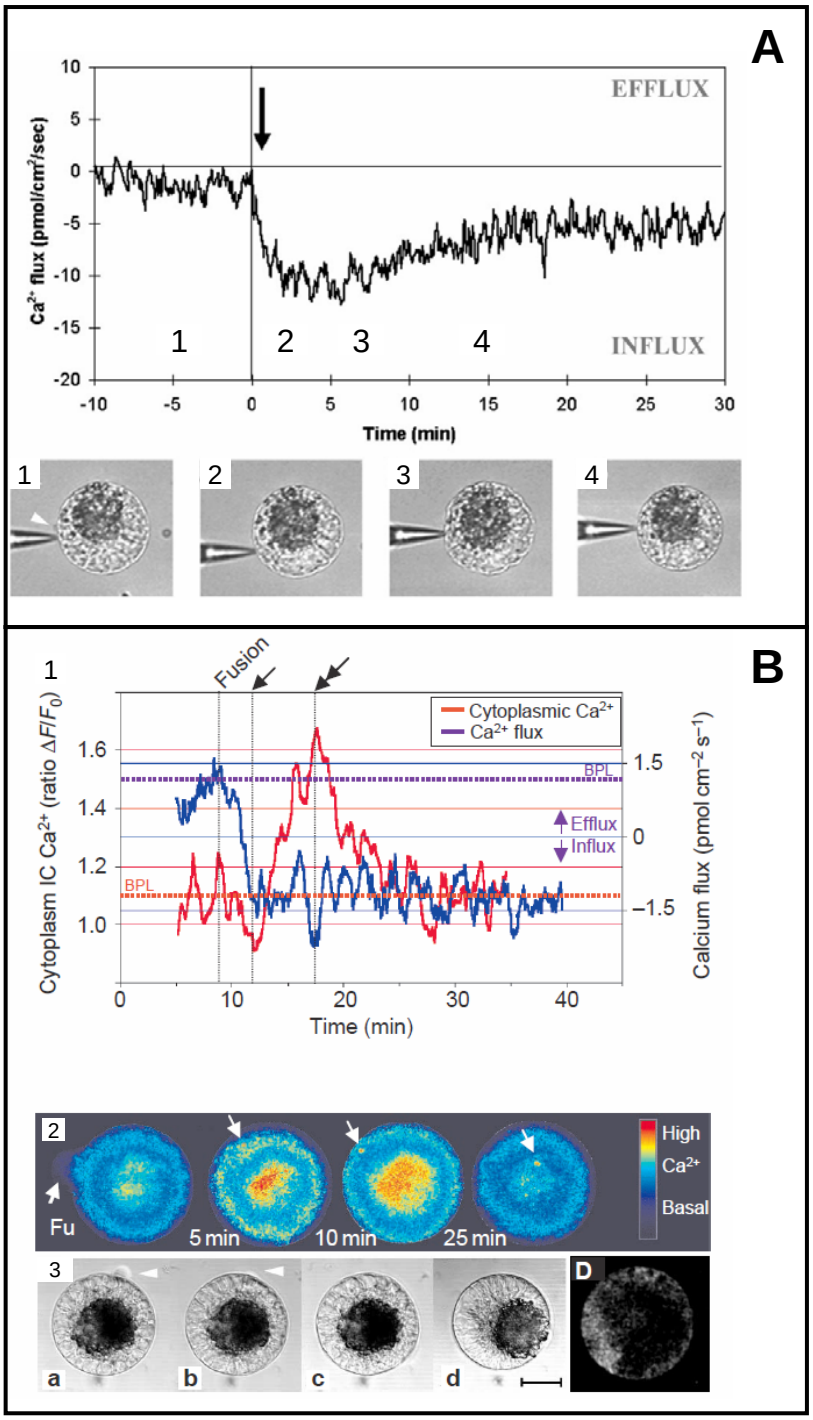
A
EFFLUX
INFLUX
Ca2+ flux (pmol/cm2/sec)
Time (min)
1
2
3
4
B
Fusion
Cytoplasmic Ca2+
Ca2+ flux
BPL
Efflux
Influx
Cytoplasm IC Ca2+ (ratio ΔF/F0)
Calcium flux (pmol cm−2 s−1)
Time (min)
Fu
5 min
10 min
25 min
High
Ca2+
Basal
D